

# Erythromyeloid progenitors give rise to a population of osteoclasts that contribute to bone homeostasis and repair

Yasuhito Yahara<sup>1,2</sup>, Tomasa Barrientos<sup>1</sup>, Yuning J. Tang<sup>1,3</sup>, Vijitha Puvindran<sup>1</sup>, Puvindran Nadesan<sup>1</sup>, Hongyuan Zhang<sup>1,4</sup>, Jason R. Gibson<sup>5</sup>, Simon G. Gregory<sup>5</sup>, Yarui Diao<sup>1,4</sup>, Yu Xiang<sup>4</sup>, Yawar J. Qadri<sup>6</sup>, Tomokazu Souma<sup>ID 7</sup>, Mari L. Shinohara<sup>ID 8,9</sup> and Benjamin A. Alman<sup>ID 1\*</sup>

Osteoclasts are multinucleated cells of the monocyte/macrophage lineage that degrade bone. Here, we used lineage tracing studies—labelling cells expressing *Cx3cr1*, *Csf1r* or *Flt3*—to identify the precursors of osteoclasts in mice. We identified an erythromyeloid progenitor (EMP)-derived osteoclast precursor population. Yolk-sac macrophages of EMP origin produced neonatal osteoclasts that can create a space for postnatal bone marrow haematopoiesis. Furthermore, EMPS gave rise to long-lasting osteoclast precursors that contributed to postnatal bone remodelling in both physiological and pathological settings. Our single-cell RNA-sequencing data showed that EMP-derived osteoclast precursors arose independently of the haematopoietic stem cell (HSC) lineage and the data from fate tracking of EMP and HSC lineages indicated the possibility of cell-cell fusion between these two lineages. *Cx3cr1*<sup>+</sup> yolk-sac macrophage descendants resided in the adult spleen, and parabiosis experiments showed that these cells migrated through the bloodstream to the remodelled bone after injury.

Bone is a multifunctional organ that not only sustains the vertebrate skeleton but also provides mineral storage and space for haematopoiesis throughout life. Bone tissue is remodelled continuously to maintain its structure and adapt to the changing environment. Bone remodelling is driven by a balance of cells that degrade and produce bone<sup>1</sup>. Osteoblasts and osteocytes have an essential role in the production of mineralized bone and are derived from mesenchymal precursors or skeletal stem cells<sup>2–4</sup>. Osteoclasts are involved in the resorption of bone tissue and are cells of the monocyte/macrophage lineage<sup>5,6</sup> that differentiate from precursors under the influence of receptor activator of NF- $\kappa$ B ligand (RANKL)<sup>7,8</sup> and undergo cell fusion to form a multinucleated cell<sup>9,10</sup>.

Cells of monocyte/macrophage lineage can differentiate from several precursors, and the different precursors give rise to distinct tissue-specific populations of macrophages. HSCs, the yolk sac or cells in the fetal liver can all produce macrophages<sup>11,12</sup>. In mice, primitive haematopoiesis starts around embryonic day 7 (E7) in the blood island of the yolk sac<sup>13–17</sup>. Early EMPS appear around E7–E7.5 in the yolk sac<sup>11,18</sup> and can differentiate into colony stimulating factor 1 receptor (*Csf1r*)<sup>+</sup> yolk-sac macrophages at E8.5 (refs. <sup>14,19</sup>). This first wave of EMP development occurs in a manner that is independent of the transcriptional activator *Myb*<sup>17,20</sup>. *Myb*-independent early EMPS can develop from E8.25 and differentiate into CX3C chemokine receptor 1 (*Cx3cr1*)<sup>+</sup> yolk-sac macrophages at E8.5, which are also known as premacrophages, resulting in a source of tissue-resident macrophages<sup>21</sup>. The second wave of EMPS, which are also known as late EMPS, emerge from the yolk sac at E8.5 and migrate to the fetal liver, resulting in a source of fetal liver monocytes<sup>22</sup>.

Later in development, HSC precursors (pro-HSCs) emerge in the aorto-gonado-mesonephros region at E10.5 and differentiate into embryonic HSCs at E12.5; these embryonic HSCs later relocate to the bone marrow<sup>17</sup>. Bone marrow HSCs eventually establish the circulating monocyte-derived macrophages<sup>11</sup>.

Here we sought to identify osteoclasts derived from EMPS and investigate their contribution to postnatal bone homeostasis and remodelling. Our fate-mapping experiments and single-cell RNA-sequencing (scRNA-seq) analyses revealed that yolk-sac macrophages of EMP origin differentiate into osteoclasts during the neonatal stage, and these cells contribute to building the medullary space for interosseous haematopoiesis. Furthermore, progenies of *Cx3cr1*<sup>+</sup> yolk-sac macrophages provide long-lasting osteoclast precursors that participate in cell-cell fusion with local precursors and contribute to the postnatal bone remodelling in both the physiological and pathological settings. Parabiosis and splenectomy show that *Cx3cr1*<sup>+</sup> yolk-sac macrophage decedents that reside in the spleen of adult mice migrate to the injury site through the bloodstream and differentiate into osteoclasts, contributing to the remodelling after bone injury.

## Results

***Csf1r*<sup>+</sup> yolk-sac macrophages give rise to the neonatal osteoclasts.** To investigate the potential contribution of EMPS to the postnatal osteoclast, *Csf1r-Mer-iCre-Mer; Rosa26<sup>tdTomato</sup> (R26<sup>tdTomato</sup>)* mice were injected once with 4-hydroxytamoxifen (4OHT) at E7.5, E8.5 or E9.5, resulting in irreversible *tdTomato* expression in *Csf1r*-expressing cells and their progenies (Fig. 1a). As *Csf1r*-expressing

<sup>1</sup>Department of Orthopaedic Surgery and Regeneration Next Initiative, Duke University, Durham, NC, USA. <sup>2</sup>Department of Orthopaedic Surgery, Faculty of Medicine, University of Toyama, Toyama, Japan. <sup>3</sup>Department of Laboratory Medicine and Pathobiology, University of Toronto, Toronto, Canada. <sup>4</sup>Department of Cell Biology and Regeneration Next Initiative, Duke University School of Medicine, Durham, NC, USA. <sup>5</sup>Duke Molecular Physiology Institute, Duke University, Durham, NC, USA. <sup>6</sup>Department of Anesthesiology, Duke University Medical Center, Durham, NC, USA. <sup>7</sup>Division of Nephrology, Department of Medicine, Duke University School of Medicine, Durham, NC, USA. <sup>8</sup>Department of Immunology, Duke University School of Medicine, Durham, NC, USA. <sup>9</sup>Department of Molecular Genetics and Microbiology, Duke University School of Medicine, Durham, NC, USA. \*e-mail: ben.alman@duke.edu

macrophages in the yolk sac appear at E8.5 (refs. <sup>18,22</sup>) and peak between E9.5 and E10.5 (refs. <sup>23</sup>), induction at E8.5 labels the majority of *Csf1r*<sup>+</sup> yolk-sac macrophages and their progenies<sup>24</sup>. Induction at E9.5 labels macrophages derived from definitive myeloid progenitors that emerge later than yolk-sac macrophages. As Cre recombination peaks at 6 h and terminates 24 h after 4OHT injection<sup>24,25</sup>, induction at E7.5 barely labels the earliest cells that express *Csf1r* with tdTomato.

At postnatal day 0 (P0), we detected a few tdTomato<sup>+</sup> cells in the femur of the mice induced at E7.5 (Fig. 1b,c), whereas none were identified in mice that were not treated with 4OHT (Extended Data Fig. 1a). By contrast, induction at E8.5 and E9.5 yielded tdTomato- and V-type proton pump-3 (Vpp3)-expressing<sup>26</sup> multinucleated osteoclasts in P0 and 0.5-month-old femurs (Fig. 1e,f). In mice induced at E8.5, there were a few tdTomato<sup>+</sup> cells in the diaphysis, whereas no tdTomato<sup>+</sup> cells were identified in the metaphysis by the age of 2 weeks (Fig. 1b-d). By contrast, the number of tdTomato<sup>+</sup> cells in the metaphysis and diaphysis of the mice induced at E9.5 was diminished at 2 months of age and had disappeared by 6 months of age (Fig. 1b,c). To verify that tdTomato<sup>+</sup> multinucleated cells were osteoclasts, we counterstained the cells with tartrate-resistant acid phosphatase (TRAP; Fig. 1g). More than 80% of TRAP<sup>+</sup> cells expressed tdTomato in the femurs of the mice induced at E8.5, verifying that *Csf1r*<sup>+</sup> yolk-sac macrophages contributed to osteoclasts in the P0 femur (Fig. 1h). However, the percentage of tdTomato<sup>+</sup>TRAP<sup>+</sup> osteoclasts induced at E8.5 decreased with age and disappeared within 2 weeks of age in the metaphysis. Furthermore, tdTomato<sup>+</sup>TRAP<sup>+</sup> cells that were induced at E9.5 also decreased over time and almost disappeared within 6 months of age (Fig. 1h). In addition to the osteoclast-specific marker expression of Vpp3 and TRAP, the multinuclear nature of these cells was consistent with the notion that tdTomato<sup>+</sup>TRAP<sup>+</sup> cells are not circulating macrophages or monocytes.

**Cx3cr1<sup>+</sup> yolk-sac macrophages give rise to the osteoclasts that survive in adulthood.** EMPs give rise to fractalkine receptor Cx3cr1-expressing yolk-sac macrophages—also known as premacrophages<sup>21</sup>—at E8.5, which then colonize the whole embryo starting at E9.5 (ref. <sup>27</sup>). We next generated *Cx3cr1*<sup>creER</sup>; *R26*<sup>tdTomato</sup> mice in which we used 4OHT to pulse label *Cx3cr1*-expressing cells and their progenies<sup>28-31</sup> (Fig. 2a). There was a limited contribution of tdTomato<sup>+</sup> cells in the P0 femurs labelled at E8.5 (Fig. 2b,c) and no tdTomato expression in 4OHT untreated mice (Extended Data Fig. 2a). However, induction at E9.5 produced an abundance of tdTomato<sup>+</sup> multinucleated cells in both the metaphysis and diaphysis of P0 femurs (Fig. 2b,c,e). By the age of 2 weeks, the number of tdTomato<sup>+</sup> cells was too sparse to detect in the metaphysis of mice that were induced at E8.5 or E9.5, but tdTomato<sup>+</sup> cells were detected in the diaphysis after induction at E9.5 (Fig. 2b-d). Notably, more

than 30% of TRAP<sup>+</sup> osteoclasts expressed tdTomato in the femurs at 2 months of age in mice that were treated with 4OHT at E8.5 or E9.5 (Fig. 2f,g). At 6 months of age, tdTomato<sup>+</sup>TRAP<sup>+</sup> osteoclasts that were induced at E9.5 survived and contributed to the remodelling of the adult femurs. tdTomato<sup>+</sup> cells were also detected in other skeletal elements, such as neonatal calvaria, adult scapula and vertebral body, and they lacked expression of macrophage marker F4/80 (Extended Data Fig. 2b-d). Thus, Cx3cr1<sup>+</sup> yolk-sac macrophages of EMP origin not only give rise to the neonatal osteoclasts but also provide long-lasting osteoclasts in adult bones.

**EMPs and HSCs give rise to the postnatal osteoclasts.** To examine the contribution of HSCs to postnatal osteoclasts, we generated *Flt3*<sup>cre</sup>; *R26*<sup>tdTomato</sup> mice and analysed their femurs at E17.5, P0 and 2 months of age. The *Flt3*<sup>cre</sup>; *R26*<sup>tdTomato</sup> mice exhibited tdTomato<sup>+</sup> cells in the femur at all time points (Fig. 3a). We confirmed the absence of tdTomato expression in femurs of E17.5 Cre<sup>-</sup> littermate controls (Extended Data Fig. 3a). In *Flt3*<sup>cre</sup>; *R26*<sup>tdTomato</sup> mice, we also detected negligible mRNA expression of *cre* in E8.5 embryos compared with bone marrow cells at 2 months, indicating the non-leakiness of *Flt3*<sup>cre</sup> mice (Extended Data Fig. 3b). In addition to the expression of TRAP and Vpp3, the multinuclear nature of these cells is consistent with tdTomato<sup>+</sup>TRAP<sup>+</sup> cells being osteoclasts (Fig. 3b,c). The percentage of tdTomato<sup>+</sup>TRAP<sup>+</sup> osteoclasts to total TRAP<sup>+</sup> osteoclasts slightly increased during early bone development and reached to 94.6% in P0 and 87.2% in the femurs of 2-month-old *Flt3*<sup>cre</sup>; *R26*<sup>tdTomato</sup> mice (Fig. 3d). As *Flt3* is not expressed in yolk-sac macrophages of EMP origin<sup>19,20,32</sup>, but is expressed specifically in the HSC lineage, the overlapping percentage of tdTomato<sup>+</sup>TRAP<sup>+</sup> osteoclasts in both fate-mapping experiments suggests that cell–cell fusion between HSCs- and EMPs-derived precursors gives rise to giant multinucleated osteoclasts.

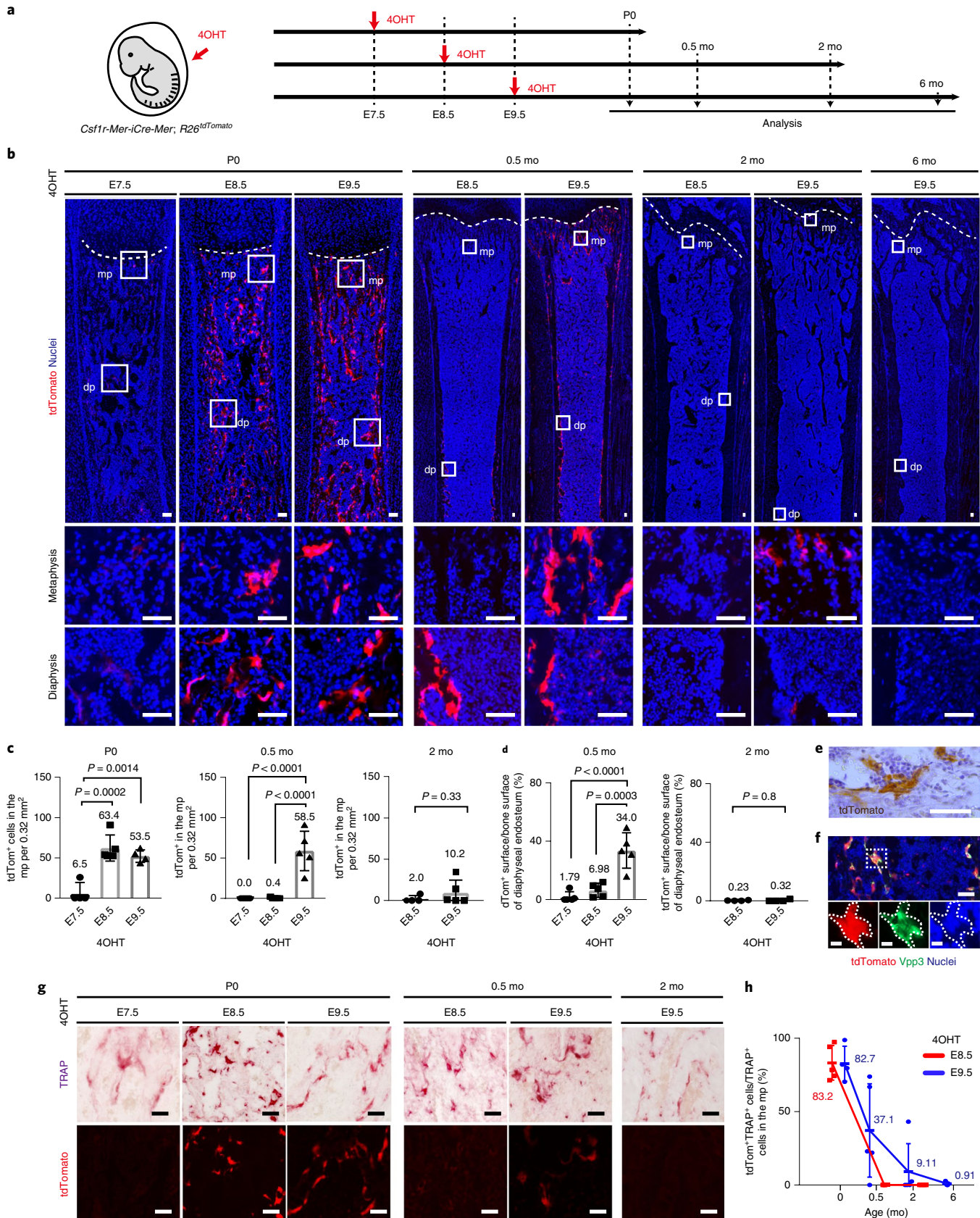
Next, we examined osteoclast precursors in the postnatal bone marrow. Negligible tdTomato<sup>+</sup> cells were identified by fluorescence-activated cell sorting (FACS) in bone marrow cells (BMCs) obtained from *Csf1r-Mer-iCre-Mer*; *R26*<sup>tdTomato</sup> and *Cx3cr1*<sup>creER</sup>; *R26*<sup>tdTomato</sup> mice induced at E8.5 or E9.5, respectively (Fig. 3e,f, Extended Data 3c). By contrast, 89.6% of CD45<sup>+</sup> BMCs from *Flt3*<sup>cre</sup>; *R26*<sup>tdTomato</sup> mice expressed tdTomato and 49.6% of them were CD11b<sup>high</sup>F4/80<sup>int</sup> monocytes rather than F4/80<sup>high</sup>CD11b<sup>int</sup> macrophages (Fig. 3e,f). Furthermore, 2.32% of CD45<sup>+</sup>tdTomato<sup>+</sup> BMCs from *Flt3*<sup>cre</sup>; *R26*<sup>tdTomato</sup> mice expressed receptor activator of NF-κB (RANK; encoded by *Tnfrsf11a*), representing a possible source of HSC-derived osteoclast precursors.

We next investigated the differentiation capacity of EMP- and HSC-derived precursors to osteoclasts in vitro. First, we isolated tdTomato<sup>+</sup> cells from a single-cell suspension of whole E14.5 embryos of *Csf1r-Mer-iCre-Mer*; *R26*<sup>tdTomato</sup> mice induced at E8.5 and *Cx3cr1*<sup>creER</sup>; *R26*<sup>tdTomato</sup> mice induced at E9.5. We found that

**Fig. 1 | *Csf1r*<sup>+</sup> yolk-sac macrophages give rise to the neonatal osteoclasts.** **a**, Schematic of the fate-mapping analysis of *Csf1r*-expressing cells and their progenies. mo, months old. **b**, Representative images of tdTomato-expressing cells in the postnatal femurs at the indicated ages and time points of 4OHT induction; P0 (E7.5,  $n=4$ ; E8.5,  $n=5$ ; E9.5,  $n=4$ ), 0.5 months old (E8.5,  $n=5$ ; E9.5,  $n=5$ ), 2 months old (E8.5,  $n=4$ ; E9.5,  $n=5$ ) and 6 months old (E9.5,  $n=4$ ). mp, metaphysis; dp, diaphysis. Scale bars, 50 μm. **c**, The number of tdTomato<sup>+</sup> cells in the metaphysis per 0.32 mm<sup>2</sup> at P0 (E7.5,  $n=4$ ; E8.5,  $n=5$ ; E9.5,  $n=4$ ), 0.5 months old (E7.5,  $n=5$ ; E8.5,  $n=5$ ; E9.5,  $n=5$ ) and 2 months old (E8.5,  $n=4$ ; E9.5,  $n=5$ ). Statistical analysis was performed using one-way analysis of variance (ANOVA; P0, 0.5 months old) and unpaired two-tailed t-tests (2 months old). tdTom<sup>+</sup>, tdTomato<sup>+</sup>. Data are mean ± s.d. **d**, The percentage of tdTomato<sup>+</sup> surface area to the total bone surface area of the endosteum at 0.5 months old (E7.5,  $n=5$ ; E8.5,  $n=5$ ; E9.5,  $n=5$ ) and 2 months old (E8.5,  $n=4$ ; E9.5,  $n=5$ ). Statistical analysis was performed using one-way ANOVA (0.5 months old) and unpaired two-tailed t-tests (2 months old). Data are mean ± s.d. **e**, Representative image of immunostaining for tdTomato indicating the multinucleation of tdTomato<sup>+</sup> cells from three independent experiments. Scale bar, 50 μm. **f**, Representative image of tdTomato expression and staining using antibodies against Vpp3. Nuclei staining with Hoechst shows the multinucleation. Three independent experiments. Scale bar, 50 μm (top); 10 μm (bottom). **g**, Representative image of tdTomato<sup>+</sup> and TRAP<sup>+</sup> cells in the postnatal femur at the indicated ages and time point of 4OHT induction; P0 (E7.5,  $n=4$ ; E8.5,  $n=5$ ; E9.5,  $n=4$ ), 0.5 months old (E8.5,  $n=5$ ; E9.5,  $n=5$ ) and 2 months old (E8.5,  $n=4$ ; E9.5,  $n=5$ ) and 6 months old (E9.5,  $n=4$ ). Scale bars, 50 μm. **h**, The percentage of tdTomato<sup>+</sup>TRAP<sup>+</sup> cells to total TRAP<sup>+</sup> cells in the metaphysis; P0 (E8.5,  $n=5$ ; E9.5,  $n=4$ ), 0.5 months old (E8.5,  $n=5$ ; E9.5,  $n=5$ ), 2 months old (E8.5,  $n=4$ ; E9.5,  $n=5$ ) and 6 months old (E9.5,  $n=4$ ). Data are mean ± s.d. For **b-d**, **g** and **h**,  $n$  represents the number of independent animals. Source data are available online.

14.2% of CD45<sup>+</sup> cells from E14.5 *Csf1r-Mer-iCre-Mer; R26<sup>tdTomato</sup>* mice expressed tdTomato; 60.5% of these tdTomato<sup>+</sup> cells were F4/80<sup>high</sup>CD11b<sup>int</sup> macrophages and 40.9% expressed RANK

(Extended Data Fig. 3d-f). By contrast, 3.19% of CD45<sup>+</sup> cells from *Cx3cr1<sup>creER</sup>; R26<sup>tdTomato</sup>* mice induced at E9.5 expressed tdTomato and a greater population of these tdTomato<sup>+</sup> cells were



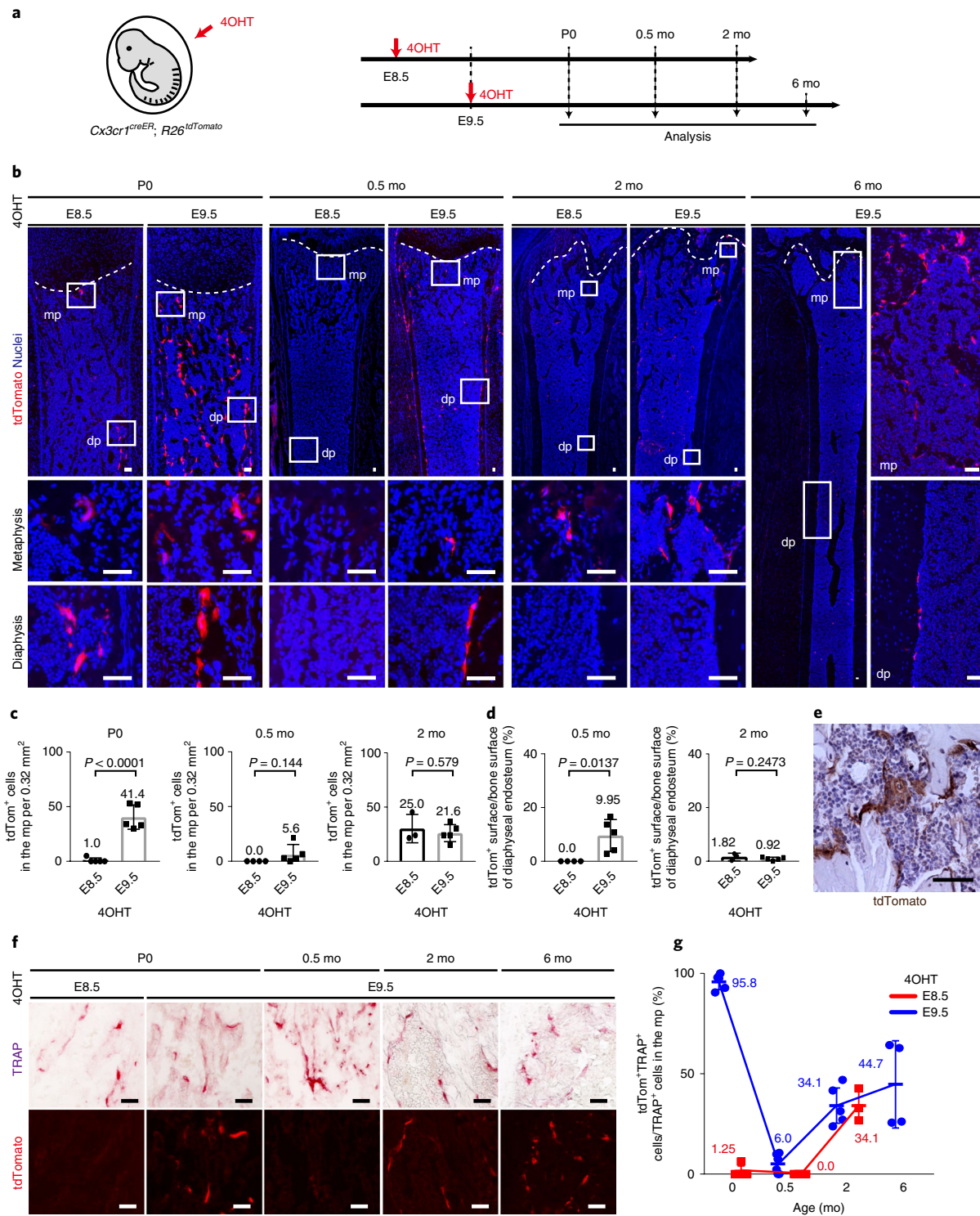


**Fig. 2 | Cx3cr1<sup>+</sup> yolk-sac macrophages give rise to the osteoclasts that survive in adulthood.** **a**, Schematic of the fate-mapping analysis of *Cx3cr1*-expressing cells and their progenies. **b**, Representative images of tdTomato<sup>+</sup> cells on postnatal femurs at P0 (E8.5,  $n=5$ ; E9.5,  $n=5$ ), 0.5 months old (E8.5,  $n=4$ ; E9.5,  $n=5$ ), 2 months old (E8.5,  $n=3$ ; E9.5,  $n=5$ ) and 6 months old (E9.5,  $n=4$ ). Scale bars, 50  $\mu$ m. **c**, The number of tdTomato<sup>+</sup> cells in the metaphysis per 0.32 mm<sup>2</sup> at P0 (E8.5,  $n=5$ ; E9.5,  $n=5$ ), 0.5 months old (E8.5,  $n=4$ ; E9.5,  $n=5$ ) and 2 months old (E8.5,  $n=3$ ; E9.5,  $n=5$ ). Statistical analysis was performed using unpaired two-tailed t-tests. Data are mean  $\pm$  s.d. **d**, The percentage of tdTomato<sup>+</sup> surface area to the total bone surface area of the endosteum at 0.5 months old (E8.5,  $n=4$ ; E9.5,  $n=5$ ) and 2 months old (E8.5,  $n=3$ ; E9.5,  $n=5$ ). Statistical analysis was performed using unpaired two-tailed t-tests. Data are mean  $\pm$  s.d. **e**, Representative image of immunostaining for tdTomato, indicating the multinucleation of tdTomato<sup>+</sup> cells. Three independent experiments were performed. Scale bar, 50  $\mu$ m. **f**, Representative images of tdTomato<sup>+</sup> and TRAP<sup>+</sup> cells on postnatal femurs at the indicated ages and time points of 4OHT induction (E8.5: P0,  $n=5$ ; E9.5: P0,  $n=5$ ; 0.5 months old,  $n=5$ ; 2 months old,  $n=5$ ; 6 months old,  $n=4$ ). Scale bars, 50  $\mu$ m. **g**, The percentage of tdTomato<sup>+</sup>TRAP<sup>+</sup> cells to total TRAP<sup>+</sup> cells in the metaphysis (E8.5: P0,  $n=5$ ; 0.5 months old,  $n=4$ ; 2 months old,  $n=3$ ; E9.5: P0,  $n=5$ ; 0.5 months old,  $n=5$ ; 2 months old,  $n=5$ ; 6 months old,  $n=4$ ). Data are mean  $\pm$  s.d. For **b-d**, **f** and **g**,  $n$  represents the number of independent animals. Source data are available online.

F4/80<sup>high</sup>CD11b<sup>int</sup> macrophages (91.8%) and RANK<sup>+</sup> cells (69.2%). We next cultured tdTomato<sup>+</sup> cells from E14.5 embryos of *Csf1r-Mer-iCre-Mer; R26<sup>tdTomato</sup>* mice (treated with 4OHT at E8.5) and *Cx3cr1<sup>creER</sup>; R26<sup>tdTomato</sup>* mice (treated with 4OHT at E9.5) and differentiated the cells into osteoclasts under stimulation with macrophage colony stimulating factor (M-CSF) and soluble RANKL<sup>33</sup>. We also cultured BMCs from 2-month-old *Flt3<sup>cre</sup>; R26<sup>tdTomato</sup>* and C57BL/6J mice and differentiated them into osteoclasts. All of these types of cells were equally capable of differentiating into tdTomato<sup>+</sup>TRAP<sup>+</sup> multinucleated osteoclasts in vitro (Fig. 3g,h).

**EMP-derived osteoclast precursors arise independently from HSC lineage.** To evaluate the possible contribution of EMP-originating yolk-sac macrophages to the postnatal osteoclast pool, we performed scRNA-seq on developing embryos. Single-cell suspensions of whole embryos at E14.5 from *Csf1r-Mer-iCre-Mer; Csf1r<sup>eGFP</sup>; R26<sup>tdTomato</sup>* mice induced at E8.5 and from *Cx3cr1<sup>creER</sup>; R26<sup>tdTomato</sup>* mice induced at E9.5 were investigated. Three cell populations—tdTomato<sup>+</sup>eGFP<sup>-</sup>, tdTomato<sup>+</sup>eGFP<sup>+</sup> and tdTomato<sup>-</sup>eGFP<sup>+</sup>—were isolated from the whole embryo of *Csf1r-Mer-iCre-Mer; Csf1r<sup>eGFP</sup>; R26<sup>tdTomato</sup>* mice. tdTomato<sup>+</sup>Cx3cr1<sup>-</sup>, tdTomato<sup>+</sup>Cx3cr1<sup>+</sup> and tdTomato<sup>-</sup>Cx3cr1<sup>+</sup> cells were isolated from *Cx3cr1<sup>creER</sup>; R26<sup>tdTomato</sup>* mice (Extended Data Fig. 4a,b). We profiled more than 35,000 single cells pooled from four embryos using two biological replicates for each genotype. Unsupervised clustering assigned the cells into distinct 29 and 21 subpopulations from *Csf1r-Mer-iCre-Mer; Csf1r<sup>eGFP</sup>; R26<sup>tdTomato</sup>* and *Cx3cr1<sup>creER</sup>; R26<sup>tdTomato</sup>* mice, respectively (Fig. 4a,f), and the cell subpopulations were readily identified using known marker genes (Fig. 4b-d,g-i, Extended Data Fig. 4c,d)

tdTomato<sup>high</sup>Csf1r<sup>high</sup> cells from *Csf1r-Mer-iCre-Mer; Csf1r<sup>eGFP</sup>; R26<sup>tdTomato</sup>* mice, which are indicative of progenies of Csf1r<sup>+</sup> yolk-sac macrophages, were mainly present in clusters 2, 4, 8, 10, 14, 18, 22, 23 and 29 (Fig. 4a,b). These cells expressed pan-macrophage markers, such as *Adgre1* and *Aifl* (Fig. 4c). tdTomato<sup>low</sup>Csf1r<sup>high</sup> cells, which are indicative of HSC-derived monocytes/macrophages, were present in clusters 1, 3, 6, 7 and 24 (Fig. 4a,b). Genes such as *Ccr2* and *Ly6c2*, which encode monocyte makers, were expressed in these clusters (Fig. 4c). Cluster 10 was enriched for genes, such as *Spic* and *Id3*, that are known to be markers of Kupffer cells and splenic red pulp macrophages<sup>21</sup>. Although 4OHT induction at E8.5 labelled mainly yolk-sac macrophages, it also labelled other subpopulations of cells, such as Ngp<sup>+</sup>Ly6g<sup>+</sup> neutrophils (cluster 15), Alas2<sup>+</sup>HbA2<sup>+</sup> erythrocytes (cluster 27) and Pecam1<sup>+</sup>Cdh5<sup>+</sup> endothelial cells (cluster 20; Fig. 4c, Extended Data Fig. 4c). Importantly, cluster 23 was a Dcstamp<sup>+</sup>Ocstamp<sup>+</sup>Atp6v0d2<sup>+</sup>Ctsk<sup>+</sup>Mmp9<sup>+</sup> osteoclast-specific population<sup>34-38</sup>. In cells from *Cx3cr1<sup>creER</sup>; R26<sup>tdTomato</sup>* mice, tdTomato<sup>high</sup>Cx3cr1<sup>high</sup> cells were located in clusters 2, 4, 6

and 7, which represented populations of yolk-sac-derived macrophages (Fig. 4f,g). These clusters showed higher expression levels of *Mrc1*, *Lyvel1*, *C1q1*, *Trem2* and *Hexb*. By contrast, cluster 1 and 3 included Cx3cr1<sup>high</sup>tdTomato<sup>low</sup> cells that expressed high levels of *Ccr2* and *Ifitm3*, representing HSC-derived monocytes/macrophages (Fig. 4i).

To delineate the distribution of tdTomato<sup>+</sup> fate-mapping cells to HSC lineage, we quantified the number of tdTomato<sup>+</sup> cells in the Flt3<sup>+</sup> clusters. A total of 726 tdTomato<sup>+</sup> cells (7.02%) from *Csf1r-Mer-iCre-Mer; Csf1r<sup>eGFP</sup>; R26<sup>tdTomato</sup>* mice distributed to clusters 11, 12, 19 and 21 (Fig. 4e), and a total of 73 tdTomato<sup>+</sup> cells (1.08%) from *Cx3cr1<sup>creER</sup>; R26<sup>tdTomato</sup>* mice distributed to cluster 16 (Fig. 4j). Although tdTomato<sup>+</sup> cells from both mice contributed to Flt3<sup>+</sup> HSC lineage, the expression levels of Flt3 in tdTomato<sup>+</sup> cells were negligible (Extended Data Fig. 4e). These data support the notion that fate-mapped EMP-derived tdTomato<sup>+</sup> cells arose independently from Flt3<sup>+</sup> HSC lineage.

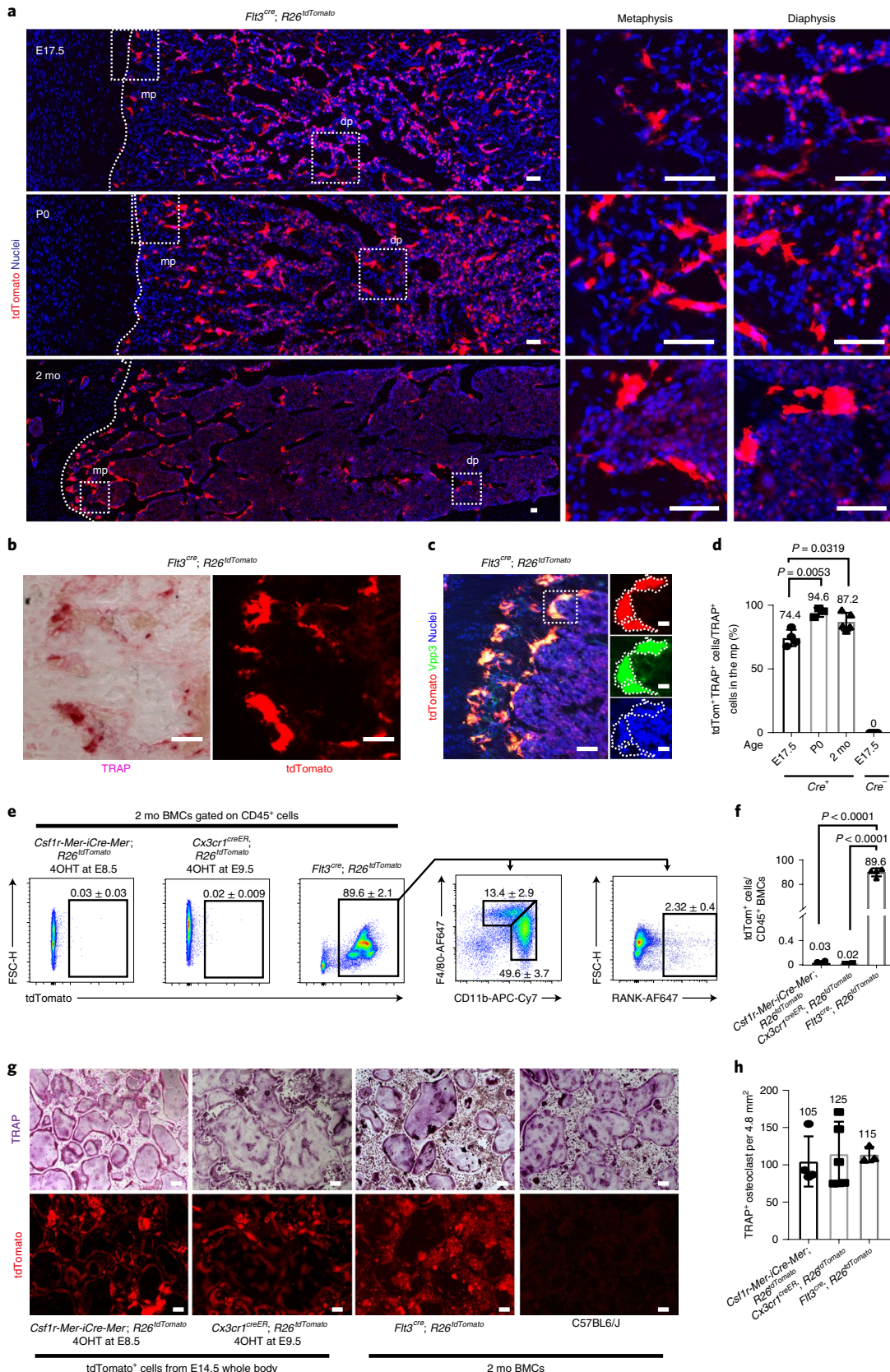
To characterize the EMP-derived osteoclast precursors, we next isolated tdTomato<sup>+</sup>Tnfrsf11a<sup>+</sup>Ptprc<sup>+</sup> cells from the data of *Csf1r-Mer-iCre-Mer; Csf1r<sup>eGFP</sup>; R26<sup>tdTomato</sup>* and *Cx3cr1<sup>creER</sup>; R26<sup>tdTomato</sup>* mice, and combined them to visualize their expression profiles. Unsupervised clustering showed 13 distinct populations (Extended Data Fig. 5a,b). Cluster 9 was an osteoclast-specific cluster, containing cells that highly express *CtsK*, *Mmp9*, *Ocstamp* and *Nfatc1*, as well as *tdTomato*, *Tnfrsf11a* and *Csf1r*, representing populations of EMP-derived mature osteoclasts (Extended Data Fig. 5a,c, Supplementary Table 1). Moreover, cells in cluster 6 expressed several genes that are related to osteoclast maturation and differentiation, such as those that encode activator protein-1 (AP-1) transcriptional factors (*Junb/d* and *Fos*)<sup>39,40</sup>, C1q complement complex (*C1qa/b/c*)<sup>41</sup>, TNF signalling pathway genes (*Tnf* and *Tnfsf9*)<sup>42</sup>, Interleukin 1 (IL-1)-mediated signalling pathway genes (*Il1a* and *Il1b*)<sup>43</sup> and Fc gamma receptors (*Fcgr3*, and *Fcgr4*)<sup>44,45</sup> (Supplementary Table 2). Pathway analysis of significantly expressed genes in cluster 6 also included several promotive osteoclast differentiation pathways as well as suppressive cytokine pathways such as IL-4, IL-12, IL-13 and IL-10 signalling<sup>46,47</sup> (Extended Data Fig. 5d). Thus, cells belonging cluster 6 were probably the source of EMP-derived osteoclast precursors.

**Cx3cr1<sup>+</sup> yolk-sac macrophage descendants provide osteoclasts after bone injury.** To examine the contribution of EMP-derived osteoclast precursors to adult bone remodelling after injury, 2-month-old *Cx3cr1<sup>creER</sup>; R26<sup>tdTomato</sup>* mice that were induced with 4OHT at E9.5 were injured by generating a drill hole in the femur<sup>48</sup> and were analysed at 3 d, 7 d, 14 d and 21 d after injury (Fig. 5a). Three days after injury, F4/80<sup>+</sup> macrophages and inflammatory cells infiltrated the injury site (Extended Data Fig. 6a,b). Serial micro-computed tomography (μCT) and histological images revealed

**Fig. 3 | EMPs and HSCs give rise to the postnatal osteoclast. a**, Representative images of tdTomato-expressing cells on femurs of *Flt3<sup>cre</sup>; R26<sup>tdTomato</sup>* mice at the indicated age ( $n=3$  mice per group). Scale bars, 50  $\mu\text{m}$ . **b**, Representative images of tdTomato<sup>+</sup> and TRAP<sup>+</sup> cells of femurs from 2-month-old *Flt3<sup>cre</sup>; R26<sup>tdTomato</sup>* ( $n=3$  mice). Scale bars, 50  $\mu\text{m}$ . **c**, Representative image of tdTomato expression and staining with antibodies against Vpp3. Nuclei staining with Hoechst shows the multinucleation. Three independent experiments were performed. Scale bar, 50  $\mu\text{m}$  (left); 10  $\mu\text{m}$  (right). **d**, Quantification of the percentage of tdTomato<sup>+</sup>TRAP<sup>+</sup> cells to total TRAP<sup>+</sup> cells in the metaphysis of *Flt3<sup>cre</sup>; R26<sup>tdTomato</sup>* mice at E17.5 ( $n=4$  mice), PO ( $n=3$  mice) and 2 months old ( $n=5$  mice). E17.5 *R26<sup>tdTomato</sup>* mice ( $n=3$  mice) were used as a Cre<sup>-</sup> control. Statistical analysis was performed using one-way ANOVA to compare among E17.5, PO and 2-month-old *Flt3<sup>cre</sup>; R26<sup>tdTomato</sup>* mice. Data are mean  $\pm$  s.d. **e**, Flow cytometry analysis of BMCs from 2-month-old *Csf1r-Mer-iCre-Mer; R26<sup>tdTomato</sup>* and *Cx3cr1<sup>creER</sup>; R26<sup>tdTomato</sup>* mice treated with 4OHT at E8.5 or E9.5, and untreated *Flt3<sup>cre</sup>; R26<sup>tdTomato</sup>* mice ( $n=4$  mice per group). **f**, Quantification of the percentage of tdTomato<sup>+</sup> cells per CD45<sup>+</sup> BMC of 2-month-old *Csf1r-Mer-iCre-Mer; R26<sup>tdTomato</sup>*, *Cx3cr1<sup>creER</sup>; R26<sup>tdTomato</sup>* and *Flt3<sup>cre</sup>; R26<sup>tdTomato</sup>* mice ( $n=4$  mice per group). Statistical analysis was performed using one-way ANOVA. Data are mean  $\pm$  s.d. **g**, In vitro osteoclast differentiation of tdTomato<sup>+</sup> cells from E14.5 *Csf1r-Mer-iCre-Mer; R26<sup>tdTomato</sup>* mice induced at E8.5 and *Cx3cr1<sup>creER</sup>; R26<sup>tdTomato</sup>* mice induced at E9.5 (left); the images are representative of three independent experiments. Right, BMCs were isolated from 2-month-old *Flt3<sup>cre</sup>; R26<sup>tdTomato</sup>* mice and C57BL/6/J mice and differentiated into osteoclasts; the images are representative of two independent experiments. The top panels show TRAP staining and the bottom panels show tdTomato expression. Scale bars, 100  $\mu\text{m}$ . **h**, The number of multinucleated TRAP<sup>+</sup> cells per 4.8  $\text{mm}^2$ . Data were combined from two independent experiments; *Csf1r-Mer-iCre-Mer; R26<sup>tdTomato</sup>*,  $n=4$  mice; *Cx3cr1<sup>creER</sup>; R26<sup>tdTomato</sup>*,  $n=5$  mice; *Flt3<sup>cre</sup>; R26<sup>tdTomato</sup>*,  $n=3$  mice. TRAP<sup>+</sup> multinucleated cells with more than three nuclei were counted as osteoclasts. Data are mean  $\pm$  s.d. Source data are available online.

that the injury site filled with new bone within 2 weeks, and was remodelled at day 21 (Fig. 5b, Extended Data Fig. 6a). The number of TRAP<sup>+</sup> osteoclasts increased at day 7, and their numbers peaked on day 14 (Fig. 5c,d). tdTomato<sup>+</sup>TRAP<sup>+</sup> cells began to increase after

day 7, with larger numbers at day 14 (Fig. 5e,f,h). About 35% of TRAP<sup>+</sup> cells coexpressed tdTomato<sup>+</sup> at day 14, indicating that EMP-derived osteoclasts contributed to the bone remodelling after injury (Fig. 5g). The tdTomato<sup>+</sup>TRAP<sup>+</sup> cells were multinucleated giant



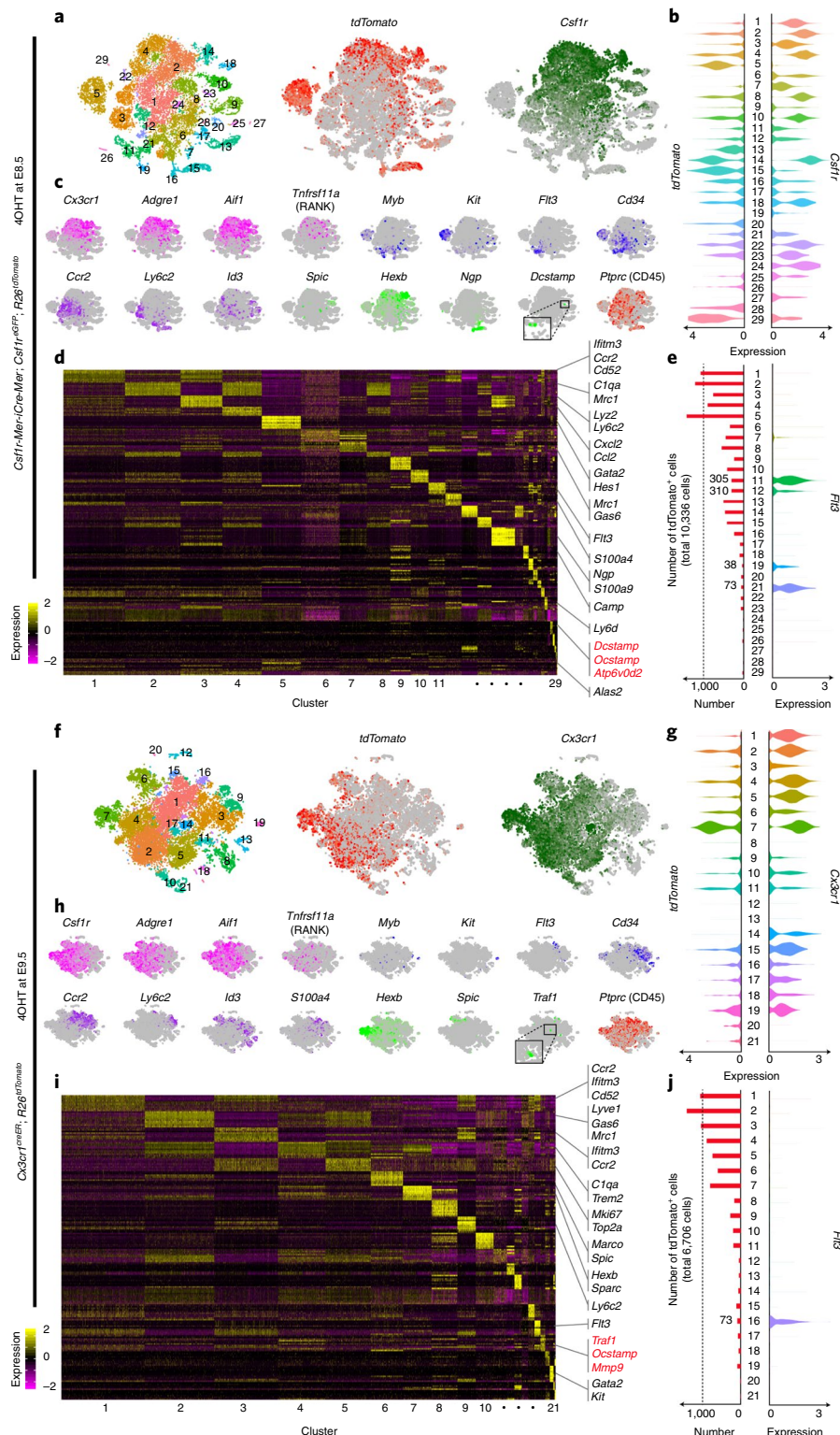


**Fig. 4 | EMP- and HSC-derived cells specify distinct subpopulations.** **a**, *t*-Distributed stochastic neighbour embedding (*t*-SNE) plots of 19,598 cells from *Csf1r-Mer-iCre-Mer; Csf1r<sup>eGFP</sup>; R26<sup>tdTomato</sup>* mice ( $n=2$  mice) identified 29 clusters. **b**, *Csf1r* and *tdTomato* expression levels of the cells from *Csf1r-Mer-iCre-Mer; Csf1r<sup>eGFP</sup>; R26<sup>tdTomato</sup>* mice ( $n=2$  mice). The values in the centre show cluster identity. **c**, Normalized expression of the indicated marker genes was visualized onto *t*-SNE plots of 19,598 cells from *Csf1r-Mer-iCre-Mer; Csf1r<sup>eGFP</sup>; R26<sup>tdTomato</sup>* mice ( $n=2$  mice). **d**, A heat map representing the top ten significantly differentially expressed genes in each cluster. **e**, The number of *tdTomato*<sup>+</sup> cells in each cluster are shown with the expression level of *Flt3*. The values in the centre show cluster identity; the dashed vertical line indicates the level of 1,000. Source data are available online. **f**, *t*-SNE plots of 16,169 cells from *Cx3cr1<sup>creER</sup>; R26<sup>tdTomato</sup>* mice ( $n=2$  mice) provided 21 clusters. **g**, *Cx3cr1* and *tdTomato* expression levels of cells from *Cx3cr1<sup>creER</sup>; R26<sup>tdTomato</sup>* mice ( $n=2$  mice). The values in the centre show cluster identity. **h**, Normalized expression of the indicated marker genes was visualized onto *t*-SNE plots of 16,169 cells from *Cx3cr1<sup>creER</sup>; R26<sup>tdTomato</sup>* mice ( $n=2$  mice). **i**, A heat map representing the top ten significantly differentially expressed genes in each cluster. **j**, The number of *tdTomato*<sup>+</sup> cells in each cluster are shown with the expression level of *Flt3*. The values in the centre show cluster identity; the dashed vertical line indicates the level of 1,000. Source data are available online.

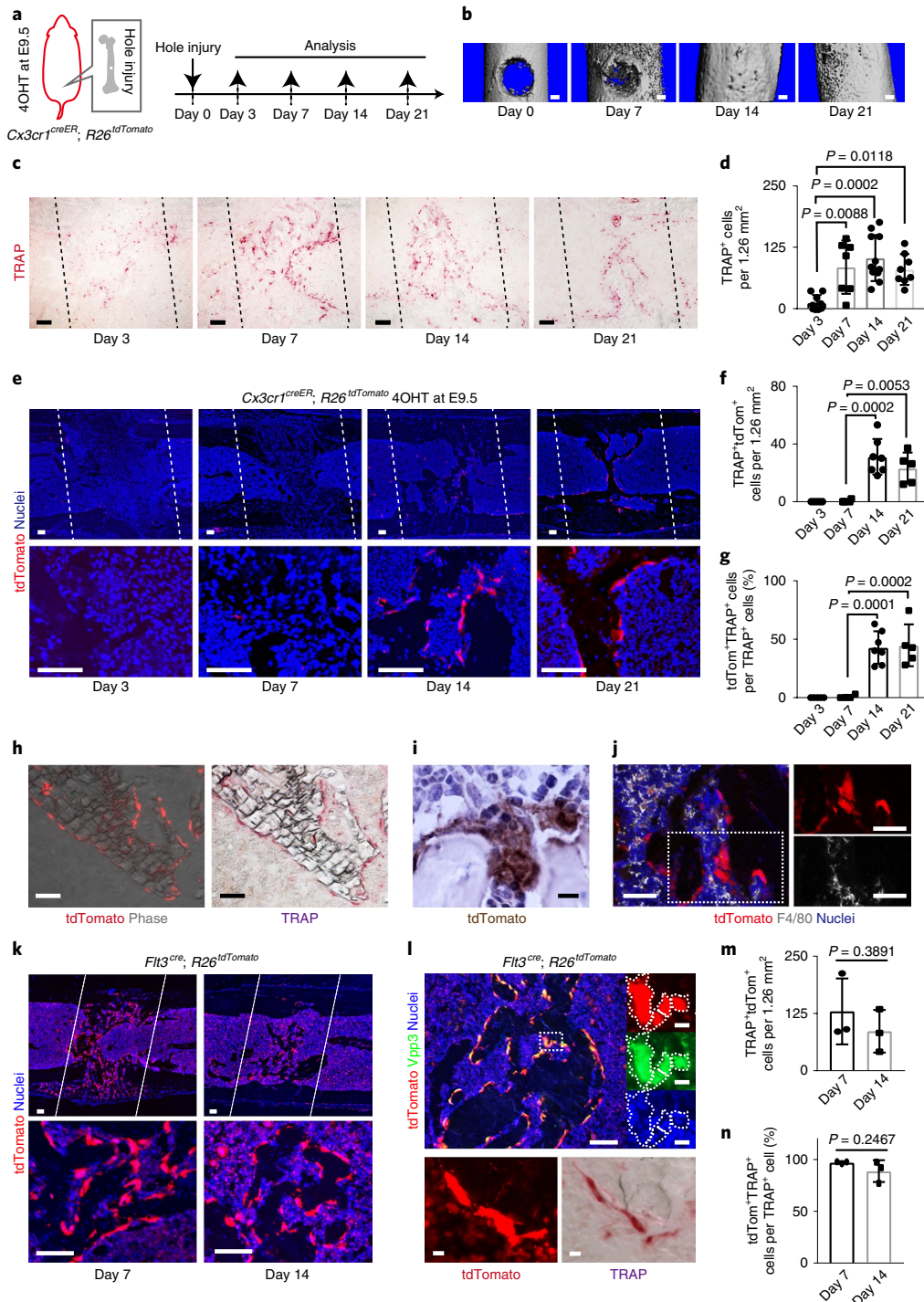


**Fig. 5 | Descendants of Cx3cr1+ yolk-sac macrophages provide osteoclasts after bone injury.** **a**, Schematic of the experimental procedure. **b**,  $\mu$ CT of the injury site during bone healing ( $n=3$  mice per group). Scale bars, 0.2 mm. **c**, TRAP staining around the injury site at days 3 ( $n=8$ ), 7 ( $n=7$ ), 14 ( $n=11$ ) and 21 ( $n=8$ ). The black dashed lines represent the site of the bone injury. Scale bars, 100  $\mu$ m. **d**, The number of TRAP<sup>+</sup> cells around the injury site per 1.26 mm<sup>2</sup> at days 3 ( $n=8$ ), 7 ( $n=7$ ), 14 ( $n=11$ ) and 21 ( $n=8$ ). Statistical analysis was performed using one-way ANOVA. Data are mean  $\pm$  s.d. **e**, tdTomato<sup>+</sup> cells around the injury site at days 3 ( $n=5$ ), 7 ( $n=4$ ), 14 ( $n=7$ ) and 21 ( $n=5$ ). The white dashed lines represent the injury site. Scale bars, 100  $\mu$ m. **f,g**, The number of tdTomato<sup>+</sup>TRAP<sup>+</sup> cells (**f**) and the percentage of tdTomato<sup>+</sup>TRAP<sup>+</sup> cells per TRAP<sup>+</sup> cell (**g**) around the injury site per 1.26 mm<sup>2</sup> at days 3 ( $n=5$ ), 7 ( $n=4$ ), 14 ( $n=7$ ) and 21 ( $n=5$ ). Statistical analysis was performed using one-way ANOVA. Data are mean  $\pm$  s.d. **h**, tdTomato<sup>+</sup> and TRAP<sup>+</sup> cells around the injury site at day 21 ( $n=5$  mice). Scale bars, 100  $\mu$ m. Phase, phase contrast. **i**, Multinucleated tdTomato<sup>+</sup> cells around the injury site at day 14;  $n=3$  mice. Scale bar, 10  $\mu$ m. **j**, F4/80 and tdTomato expression around the injury site at day 14;  $n=3$  mice. Scale bars, 50  $\mu$ m. **k**, tdTomato<sup>+</sup> cells of 2-month-old *Flt3<sup>cre</sup>; R26<sup>tdTomato</sup>* mice around the injury site;  $n=3$  mice per group. Bottom, a magnified view. The white dashed lines represent the injury site. Scale bars, 100  $\mu$ m. **l**, TRAP staining, tdTomato expression and staining with antibodies against Vpp3 at day 14. Nuclei staining with Hoechst shows the multinucleation;  $n=3$  mice. Scale bars, 100  $\mu$ m (top left); 10  $\mu$ m (top right); 10  $\mu$ m (bottom). **m,n**, The number of tdTomato<sup>+</sup>TRAP<sup>+</sup> cells (**m**) and percentage of tdTomato<sup>+</sup>TRAP<sup>+</sup> cells (**n**) per TRAP<sup>+</sup> cells around the injury site per 1.26 mm<sup>2</sup> ( $n=3$  mice per group) of *Flt3<sup>cre</sup>; R26<sup>tdTomato</sup>* mice. Statistical analysis was performed using unpaired two-tailed t-tests. Data are mean  $\pm$  s.d. For **c-g**,  $n$  represents the number of independent animals. Source data are available online.

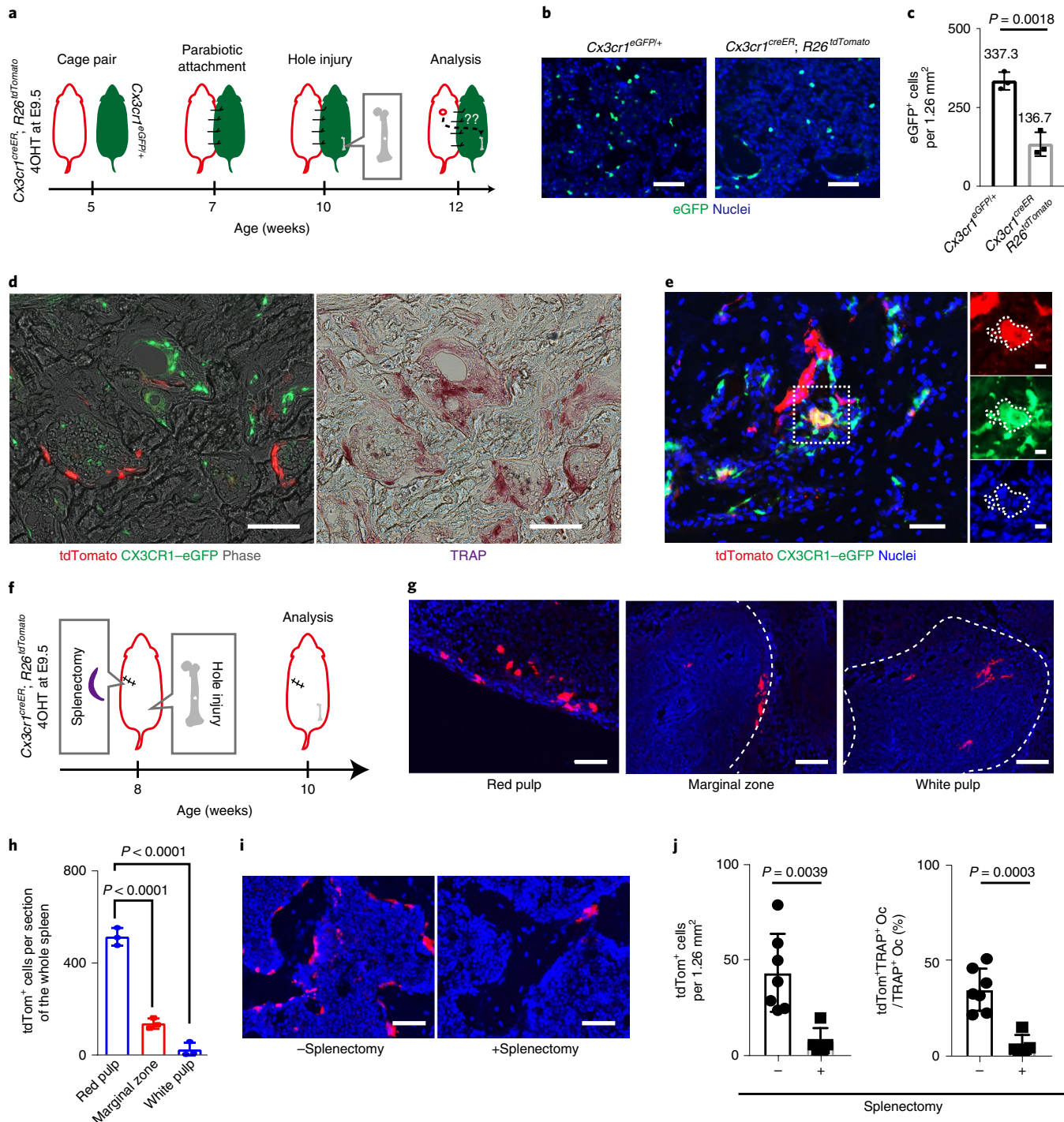


**Fig. 6 | Descendants of Cx3cr1+ yolk-sac macrophages migrated into a bone injury site through the blood circulation.** **a**, Schematic of the experimental procedure. **b**, Representative images of eGFP expression of the BMCs 5 weeks after parabiotic combination between *Cx3cr1<sup>eGFP+</sup>* and *Cx3cr1<sup>creER</sup>; R26<sup>tdTomato</sup>* mice induced with 4OHT at E9.5;  $n=3$  mice per group. Scale bars, 50  $\mu$ m. **c**, The number of eGFP+ cells per 1.26 mm<sup>2</sup>;  $n=3$  mice per group. Statistical analysis was performed using unpaired two-tailed *t*-tests. Data are mean  $\pm$  s.d. **d**, Representative images of tdTomato+ and eGFP+ cells around the injury site of *Cx3cr1<sup>eGFP+</sup>* mice 14 d after surgery;  $n=4$  independent parabiotic pairs. Left, tdTomato+ and eGFP+ cells. Right, TRAP+ cells around the injury. Scale bars, 50  $\mu$ m. **e**, Representative images of tdTomato and eGFP expression around the injury site of *Cx3cr1<sup>eGFP+</sup>* mice at day 14 showing coexpression of tdTomato and eGFP. Nuclei staining with Hoechst shows the multinucleation. Two out of four independent parabiotic pairs showed coexpression of tdTomato and eGFP in injured *Cx3cr1<sup>eGFP+</sup>* mice. Scale bars, 50  $\mu$ m (left); 10  $\mu$ m (right). **f**, Schematic of the experimental procedure. **g**, Representative images of tdTomato+ cells in the red pulp, marginal zone and white pulp of the spleen of 2-month-old *Cx3cr1<sup>creER</sup>; R26<sup>tdTomato</sup>* mice labelled at E9.5;  $n=3$  mice per group. The white dashed lines represent the boundary between the red and white pulps. Scale bars, 50  $\mu$ m. **h**, The number of tdTomato+ cells in the red pulp, marginal zone and white pulp of the spleen;  $n=3$  mice per group. Statistical analysis was performed using one-way ANOVA. Data are mean  $\pm$  s.d. **i**, Representative images of tdTomato+ cells around the injury site 14 d after injury with ( $n=5$  mice) or without ( $n=7$  mice) splenectomy. Scale bars, 50  $\mu$ m. **j**, Quantitative analysis of tdTomato+ and TRAP+ cells around the injury site 14 d after injury with ( $n=5$  mice) or without ( $n=7$  mice) splenectomy. Statistical analysis was performed using unpaired two-tailed *t*-tests. Oc, osteoclast. Data are mean  $\pm$  s.d. Source data are available online.

cells (Fig. 6*i*) but lacked expression of F4/80 (Fig. 5*j*), indicating that these cells were osteoclasts rather than macrophages/monocytes.

We also analysed 2-month-old *Csf1r-Mer-iCre-Mer; R26<sup>tdTomato</sup>* mice that were induced at E9.5; we detected a few *tdTomato*<sup>+</sup> cells in the bone marrow of these mice (Extended Data Fig. 6*c*). However, the contribution of *tdTomato*<sup>+</sup> cells to TRAP<sup>+</sup> osteoclasts was negligible (Extended Data Fig. 6*d,e*).

Next, we analysed *Flt3<sup>cre</sup>; R26<sup>tdTomato</sup>* mice 7 d and 14 d after the drill hole injury (Fig. 5*k*). Fate-mapping data showed that *tdTomato*<sup>+</sup> multinucleated cells coexpressed TRAP and Vpp3, representing osteoclasts of HSC origin (Fig. 5*l*). HSC-derived osteoclasts had already migrated to the injury site at day 7 and provided *tdTomato*<sup>+</sup>TRAP<sup>+</sup> osteoclasts around the injury site (Fig. 5*m*). The overlapping distribution of EMP-derived (Fig. 5*g*; 35.1%) and HSC-derived (Fig. 5*n*; 90.0%) *tdTomato*<sup>+</sup>TRAP<sup>+</sup> osteoclasts at day 14 indicates the possibility of cell–cell fusion between cells of EMP and HSC lineage.

**Descendants of *Cx3cr1*<sup>+</sup> yolk-sac macrophages can migrate to bone injury sites through blood circulation from a reservoir in the spleen.** Cells from EMP-derived osteoclast precursors can migrate from proliferating cells adjacent to the bone injury or through a peripheral source in the circulation. Immunostaining for Ki67 showed that *tdTomato*<sup>+</sup> cells have low proliferation potential (Extended Data Fig. 7*a,b*), raising the possibility that these cells migrated through the circulation to the injury site from a distal source. To determine the source of these cells, a parabiotic union<sup>49</sup> was achieved between *Cx3cr1*<sup>eGFP/+</sup> and *Cx3cr1*<sup>creER</sup>, *R26<sup>tdTomato</sup>* mice that were induced at E9.5. Then, 3 weeks after parabiosis, a bone injury was generated in the *Cx3cr1*<sup>eGFP/+</sup> mice and the injury site was analysed 2 weeks after surgery (Fig. 6*a*). Migration of eGFP<sup>+</sup> cells into the *Cx3cr1*<sup>creER</sup>, *R26<sup>tdTomato</sup>* mice showed effective blood sharing between two mice (Fig. 6*b,c*). A population of *tdTomato*<sup>+</sup> cells was observed at the bone injury site in *Cx3cr1*<sup>eGFP/+</sup> mice and some of these *tdTomato*<sup>+</sup> cells coexpressed TRAP (Fig. 6*d*). We also found *tdTomato*- and eGFP-double-positive multinucleated cells at the injury site (Fig. 6*e*). These data support our hypothesis that a migrating EMP-derived *tdTomato*<sup>+</sup> cell can fuse with local eGFP<sup>+</sup> cell, giving rise to a multinucleated osteoclast that contributes to bone remodelling after injury. The number of *tdTomato*<sup>+</sup> cells in the contralateral femur was significantly lower than that of the injured femur (Extended Data Fig. 7*c–e*). Thus, descendants of *Cx3cr1*<sup>+</sup> yolk-sac macrophages were able to migrate through the bloodstream and differentiate into osteoclasts, possibly fusing with local cells.

The spleen serves as a reservoir of osteoclast precursors in adult animals<sup>50</sup>. We therefore investigated whether the spleen could be a source of EMP-derived cells that could provide osteoclasts at the site of a bone injury. We performed a splenectomy and damaged the bone using drill hole surgery in *Cx3cr1*<sup>creER</sup>, *R26<sup>tdTomato</sup>* mice that were induced at E9.5 (Fig. 6*f*). *tdTomato*<sup>+</sup> cells in the spleen of *Cx3cr1*<sup>creER</sup>, *R26<sup>tdTomato</sup>* mice mainly distributed in the red pulp (Fig. 6*g,h*), consistent with a previous report showing that macrophages in the red pulp partially originate from primitive yolk sac<sup>51,52</sup>. We found that the number of *tdTomato*<sup>+</sup> cells and *tdTomato*<sup>+</sup>TRAP<sup>+</sup> osteoclasts were substantially decreased in mice that underwent a splenectomy (Fig. 6*i,j*). These data suggest the possibility that the spleen can be a pool of EMP-derived osteoclast precursors.

## Discussion

Here we investigated the origin of postnatal osteoclasts. We found that the majority of osteoclasts in neonatal bones are derived from yolk-sac macrophages of EMP origin. These cells probably participate in cell–cell fusion with HSC lineage precursors. We also found that *Cx3cr1*<sup>+</sup> yolk-sac macrophage descendants uniquely give rise to long-lasting osteoclast precursors and provide osteoclasts in adult bone. Those EMP-derived precursors can migrate to the injury site through the bloodstream and can fuse with local precursors to

create multinucleated giant osteoclasts, contributing to bone remodelling after injury (Extended Data Fig. 8).

Jacome-Galarza et al. showed that osteoclasts of EMP origin are required for normal bone development and tooth eruption<sup>32</sup>. However, the contribution of these embryonic osteoclast precursors to postnatal bone development and bone remodelling remains unclear. Our data from fate mapping, scRNA-seq and a bone injury model suggest that progenies of *Cx3cr1*<sup>+</sup> yolk-sac macrophages arise independently from the HSC lineage and can produce long-lasting osteoclasts, whereas *Csf1r*<sup>+</sup> precursors could not. One explanation for this finding is that a specific population of *Cx3cr1*<sup>+</sup> cells at E9.5 provide the long-lasting osteoclasts. The other possibility is that the production of long-lasting osteoclasts is dependent in part on the Cre recombination ability of *Csf1r-Mer-iCre-Mer* and *Cx3cr1*<sup>creER</sup> mice.

In bone development, osteoclast precursors migrate to the mesenchyme surrounding the bone rudiments. They differentiate into TRAP<sup>+</sup> cells and change into mature osteoclasts to curve the bone matrix and generate space for haematopoiesis<sup>53</sup>. EMP-derived osteoclasts play a crucial role in the production of the bone cavity and accelerate the transfer of HSCs into the bone cavity. EMP-derived osteoclasts decreased by 0.5 months of age, when this function was completed. An additional population of EMP-derived macrophages were able to survive in the body and continuously provide osteoclast precursors in mice older than 0.5 months old, representing long-lasting osteoclasts in adult mice.

We found that the spleen can be a source of EMP-derived osteoclast precursors. However, the nature of their establishment in the spleen and the biological mechanisms of response to the bone injury are still unclear. Nakamichi et al. found that IL-34 signalling induced mobilization of osteoclast precursors from the spleen in osteopetrosic op/op mice<sup>50</sup>. Furthermore, Sabatel et al. reported that lung interstitial macrophages arise from splenic reservoir monocytes through IL-10 signalling during allergic airway inflammation<sup>54</sup>. Clarification of the detailed network that orchestrates the recruitment of EMP-derived osteoclasts is required.

In summary, we found that osteoclasts are derived from EMPs and are involved in bone remodelling. Our findings provide a framework of osteoclast ontogeny and diversity of these precursor cells. Future studies into the differences between osteoclasts from these populations will inform the optimal method to modulate osteoclast functions and provide further evidence that EMP-derived osteoclasts are a unique precursor population with a specific role in bone homeostasis.

## Online content

Any methods, additional references, Nature Research reporting summaries, source data, extended data, supplementary information, acknowledgements, peer review information; details of author contributions and competing interests; and statements of data and code availability are available at <https://doi.org/10.1038/s41556-019-0437-8>.

Received: 24 December 2018; Accepted: 18 November 2019;

Published online: 6 January 2020

## References

1. Frost, H. M., Vilanueva, A. R., Jett, S. & Eyring, E. Tetracycline-based analysis of bone remodelling in osteopetrosis. *Clin. Orthop. Relat. Res.* **65**, 203–217 (1969).
2. Chan, C. K. F. et al. Identification of the human skeletal stem cell. *Cell* **175**, 43–56 (2018).
3. Debnath, S. et al. Discovery of a periosteal stem cell mediating intramembranous bone formation. *Nature* **562**, 133–139 (2018).
4. Yue, R., Zhou, Bo, O., Shimada, IsseiS., Zhao, Z. & Morrison, SeanJ. Leptin receptor promotes adipogenesis and reduces osteogenesis by regulating mesenchymal stromal cells in adult bone marrow. *Cell Stem Cell* **18**, 782–796 (2016).

5. Udagawa, N. et al. Origin of osteoclasts: mature monocytes and macrophages are capable of differentiating into osteoclasts under a suitable microenvironment prepared by bone marrow-derived stromal cells. *Proc. Natl Acad. Sci. USA* **87**, 7260–7264 (1990).
6. Takahashi, N. et al. Postmitotic osteoclast precursors are mononuclear cells which express macrophage-associated phenotypes. *Dev. Biol.* **163**, 212–221 (1994).
7. Lacey, D. L. et al. Osteoprotegerin ligand is a cytokine that regulates osteoclast differentiation and activation. *Cell* **93**, 165–176 (1998).
8. Yasuda, H. et al. Osteoclast differentiation factor is a ligand for osteoprotegerin/osteoclastogenesis-inhibitory factor and is identical to TRANCE/RANKL. *Proc. Natl Acad. Sci. USA* **95**, 3597–3602 (1998).
9. Jee, W. S. & Nolan, P. D. Origin of osteoclasts from the fusion of phagocytes. *Nature* **200**, 225–226 (1963).
10. Horton, M. A., Pringle, J. A. & Chambers, T. J. When is it an osteoclast? *J. Clin. Pathol.* **38**, 596–597 (1985).
11. Italiani, P. & Boraschi, D. Development and functional differentiation of tissue-resident versus monocyte-derived macrophages in inflammatory reactions. *Results Probl. Cell Differ.* **62**, 23–43 (2017).
12. van de Laar, L. et al. Yolk sac macrophages, fetal liver, and adult monocytes can colonize an empty niche and develop into functional tissue-resident macrophages. *Immunity* **44**, 755–768 (2016).
13. Moore, M. A. & Metcalf, D. Ontogeny of the haemopoietic system: yolk sac origin of in vivo and in vitro colony forming cells in the developing mouse embryo. *Br. J. Haematol.* **18**, 279–296 (1970).
14. Hoeffel, G. & Ginhoux, F. Fetal monocytes and the origins of tissue-resident macrophages. *Cell. Immunol.* **330**, 5–15 (2018).
15. Lee, C. Z. W., Kozaki, T. & Ginhoux, F. Studying tissue macrophages in vitro: are iPSC-derived cells the answer? *Nat. Rev. Immunol.* **18**, 716–725 (2018).
16. Palis, J., Robertson, S., Kennedy, M., Wall, C. & Keller, G. Development of erythroid and myeloid progenitors in the yolk sac and embryo proper of the mouse. *Development* **126**, 5073–5084 (1999).
17. Ginhoux, F. & Guilliams, M. Tissue-resident macrophage ontogeny and homeostasis. *Immunity* **44**, 439–449 (2016).
18. Ginhoux, F. et al. Fate mapping analysis reveals that adult microglia derive from primitive macrophages. *Science* **330**, 841–845 (2010).
19. Gomez Perdiguero, E. et al. Tissue-resident macrophages originate from yolk-sac-derived erythro-myeloid progenitors. *Nature* **518**, 547–551 (2015).
20. Schulz, C. et al. A lineage of myeloid cells independent of Myb and hematopoietic stem cells. *Science* **336**, 86–90 (2012).
21. Mass, E. et al. Specification of tissue-resident macrophages during organogenesis. *Science* **353**, aaf4238 (2016).
22. Hoeffel, G. et al. C-Myb<sup>+</sup> erythro-myeloid progenitor-derived fetal monocytes give rise to adult tissue-resident macrophages. *Immunity* **42**, 665–678 (2015).
23. Perdiguer, E. G. & Geissmann, F. The development and maintenance of resident macrophages. *Nat. Immunol.* **17**, 2–8 (2016).
24. Plein, A., Fantin, A., Denti, L., Pollard, J. W. & Ruhrberg, C. Erythro-myeloid progenitors contribute endothelial cells to blood vessels. *Nature* **562**, 223–228 (2018).
25. Wilson, C. H. et al. The kinetics of ER fusion protein activation in vivo. *Oncogene* **33**, 4877–4880 (2014).
26. Romeo, S. G. et al. Endothelial proteolytic activity and interaction with non-resorbing osteoclasts mediate bone elongation. *Nat. Cell Biol.* **21**, 430–441 (2019).
27. Stremmel, C. et al. Yolk sac macrophage progenitors traffic to the embryo during defined stages of development. *Nat. Commun.* **9**, 75 (2018).
28. Goldmann, T. et al. Origin, fate and dynamics of macrophages at central nervous system interfaces. *Nat. Immunol.* **17**, 797–805 (2016).
29. Mossadegh-Keller, N. et al. Developmental origin and maintenance of distinct testicular macrophage populations. *J. Exp. Med.* **214**, 2829–2841 (2017).
30. Molawi, K. et al. Progressive replacement of embryo-derived cardiac macrophages with age. *J. Exp. Med.* **211**, 2151–2158 (2014).
31. Hagemeyer, N. et al. Transcriptome-based profiling of yolk sac-derived macrophages reveals a role for Irf8 in macrophage maturation. *EMBO J.* **35**, 1730–1744 (2016).
32. Jacome-Galarza, C. E. et al. Developmental origin, functional maintenance and genetic rescue of osteoclasts. *Nature* **568**, 541–545 (2019).
33. Takayanagi, H. et al. Induction and activation of the transcription factor NFATc1 (NFAT2) integrate RANKL signaling in terminal differentiation of osteoclasts. *Dev. Cell* **3**, 889–901 (2002).
34. Yagi, M. et al. DC-STAMP is essential for cell-cell fusion in osteoclasts and foreign body giant cells. *J. Exp. Med.* **202**, 345–351 (2005).
35. Yang, M. et al. Osteoclast stimulatory transmembrane protein (OC-STAMP), a novel protein induced by RANKL that promotes osteoclast differentiation. *J. Cell. Physiol.* **215**, 497–505 (2008).
36. Miyamoto, H. et al. Osteoclast stimulatory transmembrane protein and dendritic cell-specific transmembrane protein cooperatively modulate cell-cell fusion to form osteoclasts and foreign body giant cells. *J. Bone Miner. Res.* **27**, 1289–1297 (2012).
37. Wu, H., Xu, G. & Li, Y. P. Atp6v0d2 is an essential component of the osteoclast-specific proton pump that mediates extracellular acidification in bone resorption. *J. Bone Miner. Res.* **24**, 871–885 (2009).
38. Saftig, P. et al. Impaired osteoclastic bone resorption leads to osteopetrosis in cathepsin-K-deficient mice. *Proc. Natl Acad. Sci. USA* **95**, 13453–13458 (1998).
39. Grigoriadis, A. E. et al. c-Fos: a key regulator of osteoclast-macrophage lineage determination and bone remodeling. *Science* **266**, 443–448 (1994).
40. Ikeda, F. et al. Critical roles of c-Jun signaling in regulation of NFAT family and RANKL-regulated osteoclast differentiation. *J. Clin. Invest.* **114**, 475–484 (2004).
41. Teo, B. H., Bobryshev, Y. V., Teh, B. K., Wong, S. H. & Lu, J. Complement C1q production by osteoclasts and its regulation of osteoclast development. *Biochem. J.* **447**, 229–237 (2012).
42. Kobayashi, K. et al. Tumor necrosis factor  $\alpha$  stimulates osteoclast differentiation by a mechanism independent of the ODF/RANKL-RANK interaction. *J. Exp. Med.* **191**, 275–286 (2000).
43. Kim, J. H. et al. The mechanism of osteoclast differentiation induced by IL-1. *J. Immunol.* **183**, 1862–1870 (2009).
44. Pierce, A. M. & Lindskog, S. Evidence for capping of Fc gamma receptors on osteoclasts. *Calcif. Tissue Int.* **39**, 109–116 (1986).
45. Seeling, M. et al. Inflammatory monocytes and Fc $\gamma$  receptor IV on osteoclasts are critical for bone destruction during inflammatory arthritis in mice. *Proc. Natl Acad. Sci. USA* **110**, 10729–10734 (2013).
46. Hong, M. H., Williams, H., Jin, C. H. & Pike, J. W. The inhibitory effect of interleukin-10 on mouse osteoclast formation involves novel tyrosine-phosphorylated proteins. *J. Bone Miner. Res.* **15**, 911–918 (2000).
47. Bendixen, A. C. et al. IL-4 inhibits osteoclast formation through a direct action on osteoclast precursors via peroxisome proliferator-activated receptor  $\gamma$ 1. *Proc. Natl Acad. Sci. USA* **98**, 2443–2448 (2001).
48. He, Y. X. et al. Impaired bone healing pattern in mice with ovariectomy-induced osteoporosis: a drill-hole defect model. *Bone* **48**, 1388–1400 (2011).
49. Conboy, I. M. et al. Rejuvenation of aged progenitor cells by exposure to a young systemic environment. *Nature* **433**, 760–764 (2005).
50. Nakamichi, Y. et al. Spleen serves as a reservoir of osteoclast precursors through vitamin D-induced IL-34 expression in osteopetrotic op/op mice. *Proc. Natl Acad. Sci. USA* **109**, 10006–10011 (2012).
51. A-Gonzalez, N. & Castrillo, A. Origin and specialization of splenic macrophages. *Cell. Immunol.* **330**, 151–158 (2018).
52. Kurotaki, D., Uede, T. & Tamura, T. Functions and development of red pulp macrophages. *Microbiol. Immunol.* **59**, 55–62 (2015).
53. Blavier, L. & Delaisse, J. M. Matrix metalloproteinases are obligatory for the migration of preosteoclasts to the developing marrow cavity of primitive long bones. *J. Cell Sci.* **108**, 3649–3659 (1995).
54. Sabatel, C. et al. Exposure to bacterial CpG DNA protects from airway allergic inflammation by expanding regulatory lung interstitial macrophages. *Immunity* **46**, 457–473 (2017).

**Publisher's note** Springer Nature remains neutral with regard to jurisdictional claims in published maps and institutional affiliations.

© The Author(s), under exclusive licence to Springer Nature Limited 2020

## Methods

**Mouse strains.** All of the animals were used according to the approved protocol by the Institutional Animal Care and Use Committee of Duke University. *Csf1r-Mer-iCre-Mer* (FVB-Tg(Csf1r-cre/Esr1\*)Ijwpl/J), *Cx3cr1<sup>creER</sup>* (B6.129P2(C)-Cx3cr1<sup>tm2.1(creERT2)Jung/J</sup>), *R26<sup>tdTomato</sup>* (B6.Cg-Gt(ROSA)26Sor<sup>tm1(CAG-tdTomato)Ijzv/J</sup>), *Csf1r-eGFP* (C57BL/6-Tg(Csf1r-EGFP-NGFR/FKBP1A/TNFRSF6)2Bck/J), *Cx3cr1<sup>eGFP</sup>* (B6.129P-Cx3cr1<sup>tm1Litt/J</sup>) and C57BL/6J mice were purchased from Jackson Laboratory. *Flt3<sup>cre</sup>* mice have been described previously described<sup>55</sup> and were provided by K. Levine (Washington University). All of the mice were bred under specific-pathogen-free conditions. *Csf1r-Mer-iCre-Mer*, *Cx3cr1<sup>creER</sup>* and *Flt3<sup>cre</sup>* mice were mated with *R26<sup>tdTomato</sup>* mice to generate *Csf1r-Mer-iCre-Mer*; *R26<sup>tdTomato</sup>*, *Cx3cr1<sup>creER</sup>*; *R26<sup>tdTomato</sup>* or *Flt3<sup>cre</sup>*; *R26<sup>tdTomato</sup>* mice. In some of the experiments, *Csf1r-Mer-iCre-Mer*; *R26<sup>tdTomato</sup>* and *Csf1r-eGFP* mice were crossed to obtain *Csf1r-Mer-iCre-Mer*; *Csf1r-eGFP*; *R26<sup>tdTomato</sup>* mice. *Csf1r-Mer-iCre-Mer* mice were maintained in a mixed background of FVB and C57BL/6J. Genotyping PCR of each strain was performed according to the instructions provided by Jackson Laboratory. Embryonic development was defined on the basis of the date of vaginal plug formation, which was set as E0.5. To achieve Cre recombination, 75 µg g<sup>-1</sup> (bodyweight) of 4OHT (Sigma-Aldrich) dissolved in corn oil (Sigma-Aldrich) was intraperitoneally injected into a pregnant female. 4OHT was supplemented with 37.5 µg g<sup>-1</sup> (bodyweight) progesterone (Sigma-Aldrich) to avoid fetal abortions.

**Histological analysis.** Samples were fixed in 4% paraformaldehyde (PFA) and phosphate-buffered saline (PBS) at 4°C, and then incubated overnight in 30% sucrose in PBS (Sigma-Aldrich). The tissue samples were embedded in Tissue-Tek O.C.T. compound (Sakura Finetek). The sections were prepared at a thickness of 10 µm with a Cryofilm type 3c (16UF) (SECTION-LAB) using a CM1950 cryomicrotome (Leica) according to a previously described method<sup>56</sup>. The sections were stained with Hoechst 33342 (1:2,000, Thermo Fisher Scientific) to visualize the nuclei. tdTomato and eGFP fluorescence were captured using an Axio Imager Widefield Fluorescence Microscope (Zeiss) or a BZ-9000 Biorevo microscope (Keyence). For immunostaining of F4/80, Vpp3 and Ki67, sections were blocked with 10% normal goat serum (Vector Laboratories) in PBS for 1 h at room temperature. The sections were then incubated overnight with rat anti-mouse F4/80 (1:200, Bioworld), rabbit anti-ATP6V1B1 + ATP6V1B2 (1:200, Abcam) or rat anti-Ki67 (1:200, Thermo Fisher Scientific) antibodies at 4°C. Anti-rat Alexa Fluor 647 (1:2,000, Thermo Fisher Scientific) and anti-rabbit Alexa Fluor 488 (1:2,000, Thermo Fisher Scientific) antibodies were used as secondary antibodies. After nuclei staining with Hoechst 33342, the sections were visualized using an Axio Imager Widefield Fluorescence Microscope (Zeiss) or a IX-83 (Olympus).

For paraffin-embedded sections, samples were collected, fixed in 4% PFA, processed and embedded in paraffin. The sections were prepared at a thickness of 5 µm and stained with haematoxylin and eosin after deparaffinization. To detect tdTomato expression, sections were incubated in citric-acid-based antigen unmasking solution (Vector Laboratories) at 80°C for 15 min to retrieve the antigen. Endogenous peroxidase was blocked by 3% H<sub>2</sub>O<sub>2</sub> and methanol for 10 min. After blocking with 10% goat normal serum (Vector Laboratories), the sections were incubated with rabbit anti-RFP antibodies (1:500, Rockland) for 2 h at room temperature. Immunodetection was performed using VECTASTAIN ABC rabbit IgG kit and ImmPACT DAB peroxidase (HRP) substrate (Vector Laboratories). The sections were then counterstained with haematoxylin and mounted.

**TRAP staining.** To visualize tdTomato<sup>+</sup> and TRAP<sup>+</sup> cells, frozen sections were used as described above and previously<sup>56</sup>. First, tdTomato expression was captured using an Axio Imager Widefield Fluorescence Microscope (Zeiss) without embedding. Sections were then stained for TRAP. TRAP staining solution containing Naphthol AS-MX phosphate (Sigma-Aldrich) and Fast Red Violet LB salt (Sigma-Aldrich), diluted in L-(+)-tartaric acid (Sigma-Aldrich) incubation medium, was placed on the film and incubated at 37°C for 15 min. After washing the film, the sections were embedded with SCMM-G1 (Section-Lab) and captured using an Axio Imager Widefield Fluorescence Microscope (Zeiss). Photoshop (Adobe) was used to merge the two types of images. Quantitative histological evaluations were then performed.

**Preparation of cell suspensions, flow cytometry and cell sorting.** To obtain single-cell suspensions from E14.5 embryos, pregnant females were euthanized by exposure to CO<sub>2</sub>. Embryos were collected from the uterus and washed with PBS. Each embryo was minced using a scalpel and then digested with 1 mg ml<sup>-1</sup> collagenase D (Roche), 100 U ml<sup>-1</sup> DNase I (Sigma-Aldrich) in 1% bovine serum albumin (Sigma-Aldrich) and PBS for 20 min at 37°C. The whole-body cell suspension was filtered using 70-µm and 30-µm cell strainers. To obtain the BMCs, 2-month-old mice tibia were used. Bilateral tibia were dissected, and the distal and proximal ends of the tibia were removed. BMCs were then collected and mechanically dissociated to generate a single-cell suspension. BMCs were then filtered using a 40-µm cell strainer.

The cell suspensions were centrifuged at 1,200 r.p.m. for 5 min and then treated with ACK lysis buffer (Thermo Fisher Scientific) for 3 min. After incubation for 5 min with purified rat anti-mouse CD16/32 antibodies (Mouse BD Fc block, BD

Biosciences), antibody mixes were added and incubated for 30 min at 4°C.

A complete list of the antibodies used is provided in Supplementary Table 3. Flow cytometry was performed using a FACSCanto II flow cytometer (BD Biosciences). Data were analysed using FlowJo v.10 (Tree Star). For cell sorting, a DiVa cell sorter (BD Biosciences) was used, and the sorted cells were used for either scRNA-seq or primary osteoclast cultures.

**scRNA library preparation and sequencing.** Cell suspensions were loaded onto a 10x Genomics Chromium Controller Single-Cell Instrument (10x Genomics) mixed with reverse transcription (RT) reagents along with gel beads and oil to generate single-cell gel bead-in emulsions (GEMs). GEM-RT was performed using an Eppendorf Mastercycler Pro (Eppendorf) with the following program: 53°C for 45 min, 85°C for 5 min and then held at 4°C. After RT, GEMs were broken and the single-strand cDNA was purified using DynaBeads MyOne Silane Beads (Thermo Fisher Scientific). cDNA was then amplified using the Eppendorf Mastercycler Pro (Eppendorf) using the following program: 98°C for 3 min; 11–13 cycles of 98°C for 15 s, 67°C for 20 s and 72°C for 1 min; and then held at 4°C. The amplified cDNA product was then purified using the SPRIselect Reagent Kit (0.6 × SPRI; Beckman Coulter). Indexed sequencing libraries were constructed using the reagents in the Chromium Single-Cell Library Kit 3' v2, according to the following steps: (1) fragmentation, end repair and A-tailing; (2) SPRIselect cleanup; (3) adapter ligation; (4) post-ligation cleanup with SPRIselect; (5) sample index PCR; and (6) post-index PCR cleanup. The barcoded sequencing libraries were quantified using quantitative PCR (qPCR; KAPA Biosystems Library Quantification Kit for Illumina platforms). Sequencing libraries were transferred to the Duke University Center for Genomic and Computational Biology (GCB) and were loaded onto a Novaseq 6000 system (Illumina) for sequencing.

The primary analytical pipeline for the single-cell analysis was performed according to the recommended protocols from 10x Genomics. In brief, we processed the raw FASTQ files using the most recent version of Cell Ranger 3.0 (<http://support.10xgenomics.com/single-cell/software/pipelines/latest/what-is-cell-ranger>). The first steps of this program demultiplex the raw reads and align the reads to the appropriate reference transcriptome and gene expression matrices created for all single cells in each sample. The secondary statistical analysis was performed using R package Seurat 3.0.0.9000 (<http://satijalab.org/seurat/>), which performs quality control and subsequent analyses on the gene expression matrices produced by Cell Ranger. In Seurat, data were first normalized to a log scale after basic filtering for minimum gene and cell observance frequency cut-offs ([http://satijalab.org/seurat/pbmc3k\\_tutorial.html](http://satijalab.org/seurat/pbmc3k_tutorial.html)). We then closely examined the data and performed further filtering on the basis of a range of metrics in an attempt to identify and exclude possible multiplets. The additional removal of further technical artefacts, to reduce noise, was performed using regression methods. After quality control procedures were completed, we calculated principal components using the most variably expressed genes in our dataset. Significant principal components for downstream analyses were determined using previously described methods<sup>57</sup>, and these principal components were carried forward for two main purposes—to perform cell clustering and to enhance visualization. Cells were grouped into an optimal number of clusters for de novo cell-type discovery using the FindClusters function in Seurat—a graph-based clustering approach with visualization of cells through the use of t-SNE—which reduced the information captured in the selected significant principal components to two dimensions<sup>58</sup>. Differential expression of relevant cell marker genes was visualized on the t-SNE plot to reveal specific individual cell types.

**qPCR.** Total RNA was extracted from whole embryos at E8.5 and bone marrow cells at 2 months old using Trizol reagent (ambient) and Direct-zol RNA Microprep (Genesee Scientific). cDNA was then reverse transcribed using Maxima H Minus cDNA Synthesis Master Mix (Invitrogen, M1662). qPCR was then performed with the following primers using the Powerup SYBR green reagent (Invitrogen, A25777) on a QuantStudio 3 real-time PCR system (Thermo Fisher Scientific). Gene expression was calculated and expressed relative to a housekeeping gene (*Hprt*) using the ΔΔC<sub>t</sub> method. Cre-forward primer, ACCTTCACCGGCATCAACGT; Cre-reverse, CTGCATTACCGGTCGATGCA; *Hprt*-forward, GGCTATAAGTTCTTGCTGACCTG; and *Hprt*-reverse, AACTTTATGTCCCCGGTGA.

**Pathway analysis.** Pathway analysis was performed using the ToppGene Suite (<https://toppgene.cchmc.org/help/publications.jsp>). We used a total of 163 differentially expressed genes in cluster 6 of tdTomato<sup>+</sup>Tnfrsf11a<sup>+</sup>Ptprc<sup>+</sup> cells to identify the significantly upregulated pathways on the basis of functional annotations and a protein interactions network.

**In vitro osteoclast differentiation.** tdTomato<sup>+</sup> cells were isolated from whole-body cell suspensions of E14.5 *Csf1r-Mer-iCre-Mer*; *R26<sup>tdTomato</sup>* and *Cx3cr1<sup>relER</sup>*; *R26<sup>tdTomato</sup>* embryos and tdTomato<sup>+</sup> cells were seeded in a 48-well plate (20,000 cells per well). Cells were cultured in α-MEM (Thermo Fisher Scientific) with 20% FBS (Sigma-Aldrich) containing 50 ng ml<sup>-1</sup> M-CSF (R&D Systems) for 2 d. Cells were then cultured in the presence of 50 ng ml<sup>-1</sup> soluble RANKL (Peprotech) and 50 ng ml<sup>-1</sup> M-CSF for 3 d.

BMCs from *Flt3<sup>cre</sup>; R26<sup>tdTomato</sup>* and C57BL/6J mice were isolated and seeded in 10 cm dishes. Non-adherent BMCs were seeded (20,000 cells per well of a 48-well plate) and cultured in α-MEM with 20% FBS containing 50 ng ml<sup>-1</sup> M-CSF for 2 d. Cells were then cultured in the presence of 50 ng ml<sup>-1</sup> soluble RANKL and 50 ng ml<sup>-1</sup> M-CSF for 3 d.

Cells were fixed with 4% PFA and PBS and stained for TRAP. Multinucleated (>3 nuclei) TRAP<sup>+</sup> cells were counted as osteoclasts and were captured using a BZ-9000 Biorevo microscope (Keyence).

**Drill hole surgery.** Two-month-old mice received the drill hole surgery under anaesthesia. A 22-gauge needle (0.7 mm diameter, BD) was used to create a hole on the right femur approximately 6 mm above the knee joint without a skin incision. Mice were euthanized at 3 d, 7 d, 14 d and 21 d after surgery and analysed using μCT (VivaCT 80, Scanco Medical) and histological analysis.

**Parabiosis surgery.** Two mice were habituated in the same cage to ensure harmonious cohabitation. After the anaesthesia, a longitudinal skin incision was performed from elbow to knee joint. After a suture was applied at the olecranon, muscle and subcutaneous tissue of the two mice were connected by continuous sutures. The skin was sutured in the area from the elbow to knee joint. The mice were monitored daily to observe for signs of pain and distress, such as shaking, lethargy, chewing of the tail, arched back and lack of grooming. After a total 3 weeks combination, a mouse received a drill hole surgery on the right femur under anaesthesia. Then, 2 weeks after the drill hole surgery, the mice were euthanized and processed for histological analysis.

**Splenectomy surgery.** After anaesthesia, the abdominal cavity was exposed through a left lateral incision extending around 1 cm. Splenic vessels were collapsed using a cauterity, then the spleen was removed with scissors. The abdominal musculature and the skin were closed with suture.

**Statistical analysis and reproducibility.** Data are shown as mean ± s.d. with individual values per sample. Statistical analysis was performed using either Prism (GraphPad) or Statcel3 (OMS) using unpaired two-tailed *t*-tests and ANOVA followed by Tukey–Kramer post hoc test. *P*<0.05 was considered to be significant. All of the statistical analyses performed in this study and their respective parameters are shown in the figure legends. Source data are available online.

The number (*n*) of biological repeats is indicated in each figure legend. All representative data are shown from independently repeated experiments or independents animals with similar results.

**Reporting Summary.** Further information on research design is available in the Nature Research Reporting Summary linked to this article.

## Data availability

The scRNA-seq data that support the findings of this study have been deposited in the Gene Expression Omnibus (GEO) under accession code [GSE125088](#). Source

data are available online for Figs. 1–6 and Extended Data Figs. 3 and 5–7. All other data supporting the findings of this study are available from the corresponding author on reasonable request.

## References

55. Epelman, S. et al. Embryonic and adult-derived resident cardiac macrophages are maintained through distinct mechanisms at steady state and during inflammation. *Immunity* **40**, 91–104 (2014).
56. Kawamoto, T. Use of a new adhesive film for the preparation of multi-purpose fresh-frozen sections from hard tissues, whole-animals, insects and plants. *Arch. Histol. Cytol.* **66**, 123–143 (2003).
57. Macosko, E. Z. et al. Highly parallel genome-wide expression profiling of individual cells using nanoliter droplets. *Cell* **161**, 1202–1214 (2015).
58. van der Maaten, L. & Hinton, G. Visualizing data using t-SNE. *J. Mach. Learn. Res.* **9**, 2579–2605 (2008).

## Acknowledgements

We thank A. J. Mirando, S. Ide, E. Hocke and K. Abramson for assistance and discussions; staff at Duke Molecular Physiology Institute Molecular Genomics Core for generation and analysis of 10x Genomics scRNA-seq libraries; T. Kimura for reading the manuscript and discussion; G. S. Baht for the instruction of the parabiosis surgery. This research was supported by a grant from the National Institute on Aging (NIA) of the National Institutes of Health (NIH) R01 AG049745 and NIH R01 AI088100. The content is solely the responsibility of the authors and does not necessarily represent the official views of the NIH.

## Author contributions

Conceptualization: B.A.A. and Y.Y. Methodology: B.A.A., Y.Y., Y.J.T. and Y.J.Q. Validation: Y.J.T., P.N., V.P., H.Z. and T.B. Formal analysis: B.A.A., Y.Y., V.P., J.G., S.G.G., Y.D., Y.X. and T.S. Investigation: Y.Y., Y.J.T., P.N., V.P., J.G. and S.G.G. Resources: B.A.A. and Y.Y. Data curation: Y.Y., Y.J.T., P.N., V.P., H.Z., J.G., S.G.G. and Y.J.Q. Writing, original draft: Y.Y.; reading and editing: B.A.A., Y.J.T., Y.J.Q., M.L.S., V.P., H.Z. and S.G.G. Visualization: Y.Y. Supervision: B.A.A., T.B. and M.L.S. Project administration: B.A.A. Funding acquisition: B.A.A.

## Competing interests

The authors declare no competing interests.

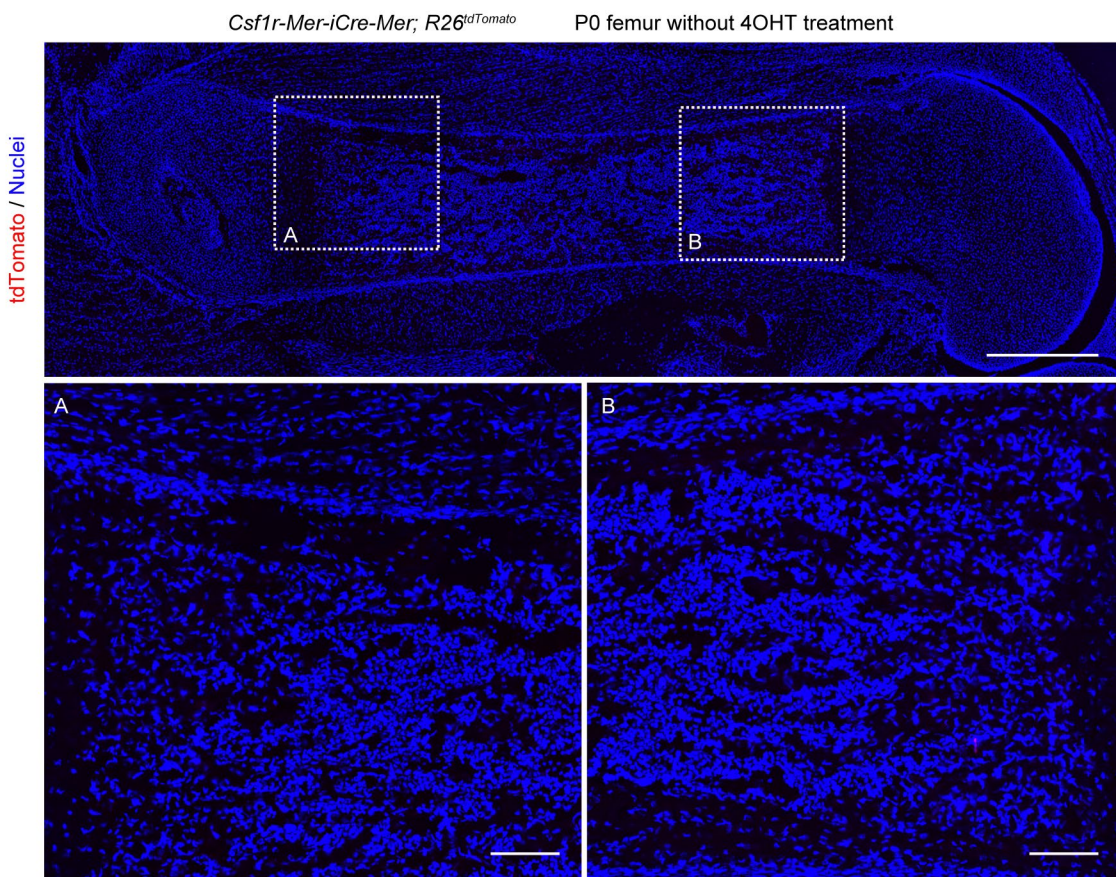
## Additional information

**Extended data** is available for this paper at <https://doi.org/10.1038/s41556-019-0437-8>.

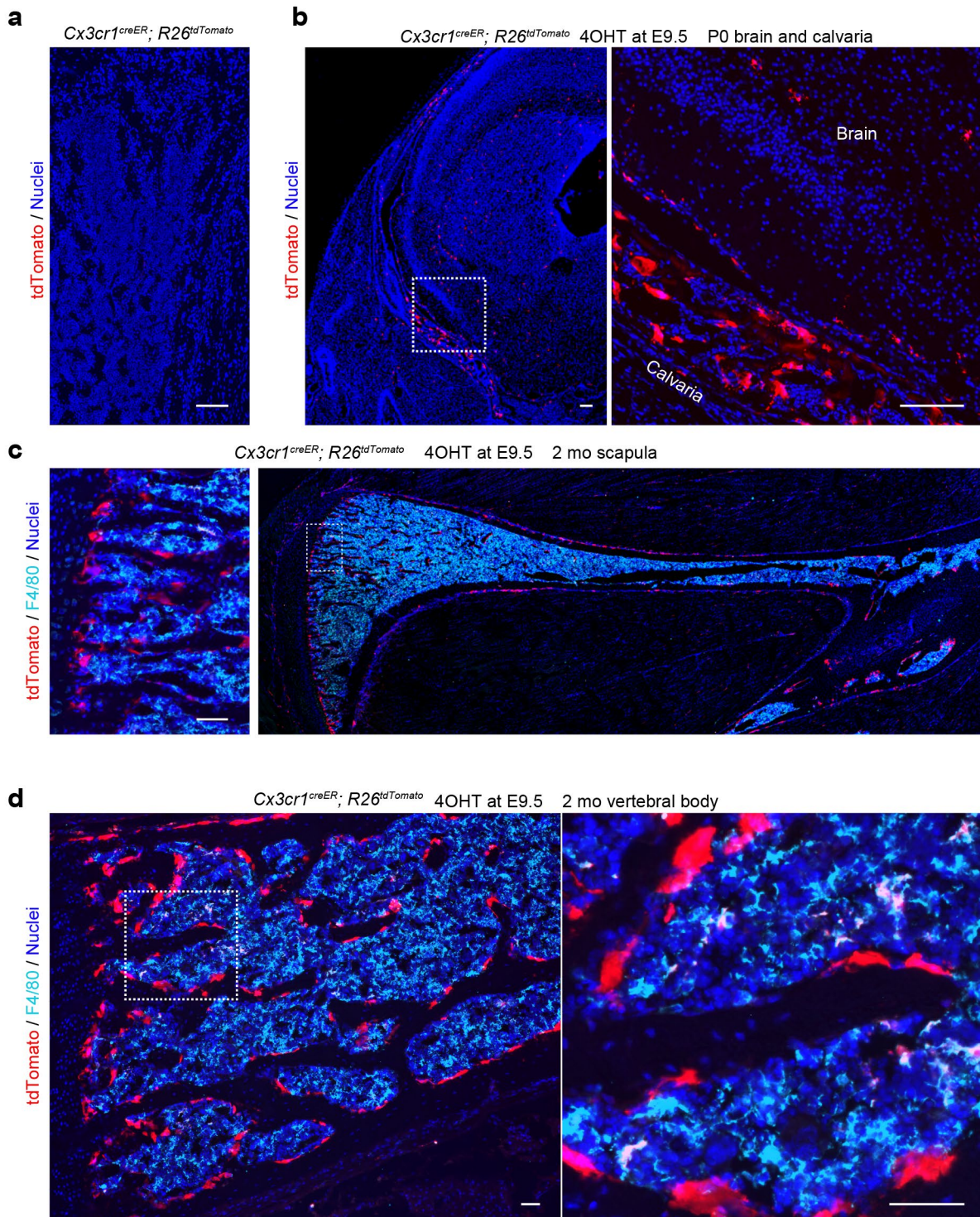
**Supplementary information** is available for this paper at <https://doi.org/10.1038/s41556-019-0437-8>.

**Correspondence and requests for materials** should be addressed to B.A.A.

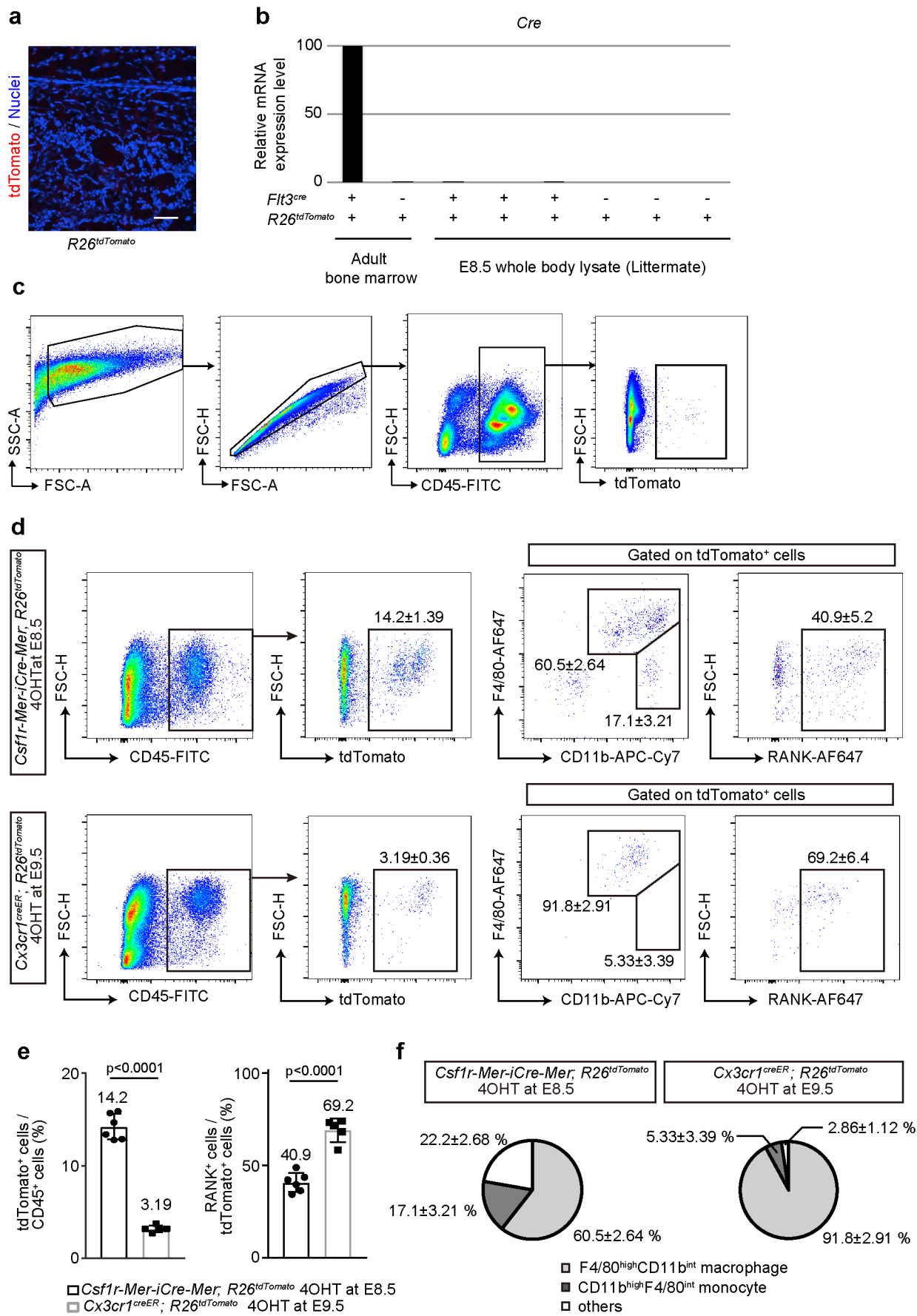
**Reprints and permissions information** is available at [www.nature.com/reprints](http://www.nature.com/reprints).

**a**

**Extended Data Fig. 1 | Non-leakiness of *Csf1r-Mer-iCre-Mer* mice.** **a**, Representative image of the postnatal day (P) 0 femur of *Csf1r-Mer-iCre-Mer; R26<sup>tdTomato</sup>* mice without 4 hydroxytamoxifen (4OHT) induction ( $n=3$  mice). Scale bars, upper panel; 500  $\mu\text{m}$ . Lower panels; 100  $\mu\text{m}$ .

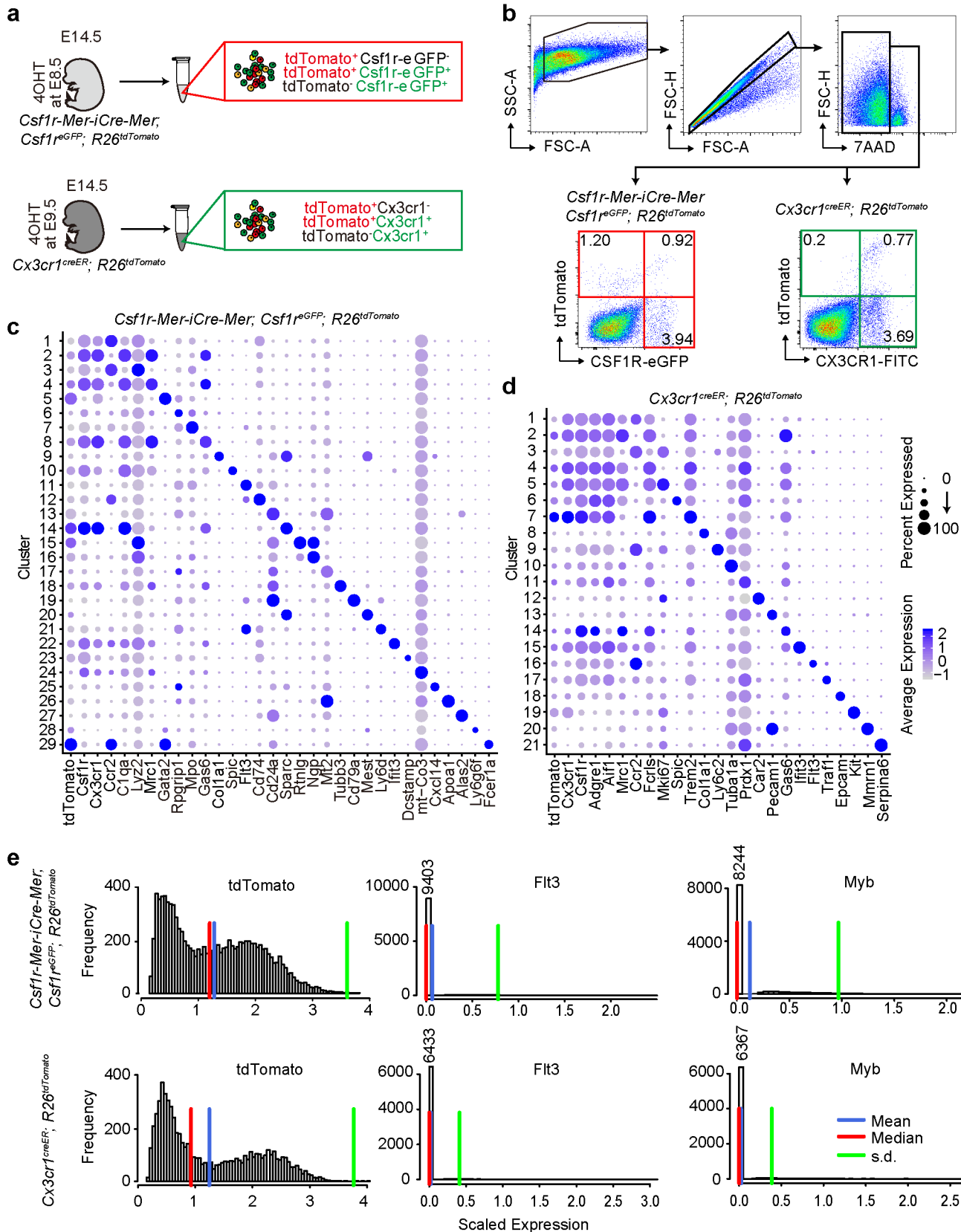


**Extended Data Fig. 2 | Cx3cr1<sup>+</sup> yolk-sac macrophage descendant in several skeletal elements.** **a**, Representative image of the postnatal day (P) 3 femur of *Cx3cr1<sup>creER</sup>; R26<sup>tdTomato</sup>* mice without 4-hydroxytamoxifen (4OHT) induction (n=3 mice). Scale bar, 100  $\mu$ m. **b**, Representative images of tdTomato<sup>+</sup> cells in neonatal brain and calvaria of *Cx3cr1<sup>creER</sup>; R26<sup>tdTomato</sup>* mice treated with 4OHT at E9.5 (n=3 mice). Scale bars, 50  $\mu$ m. **c**, Representative image of tdTomato and F4/80 expression in the scapula of 2-month-old (mo) *Cx3cr1<sup>creER</sup>; R26<sup>tdTomato</sup>* mice labeled at E9.5 (n=3 mice). Scale bar, 50  $\mu$ m. **d**, Representative image of tdTomato and F4/80 expression in the vertebral body of 2 mo *Cx3cr1<sup>creER</sup>; R26<sup>tdTomato</sup>* mice labeled at E9.5 (n=3 mice). Scale bars, 50  $\mu$ m.



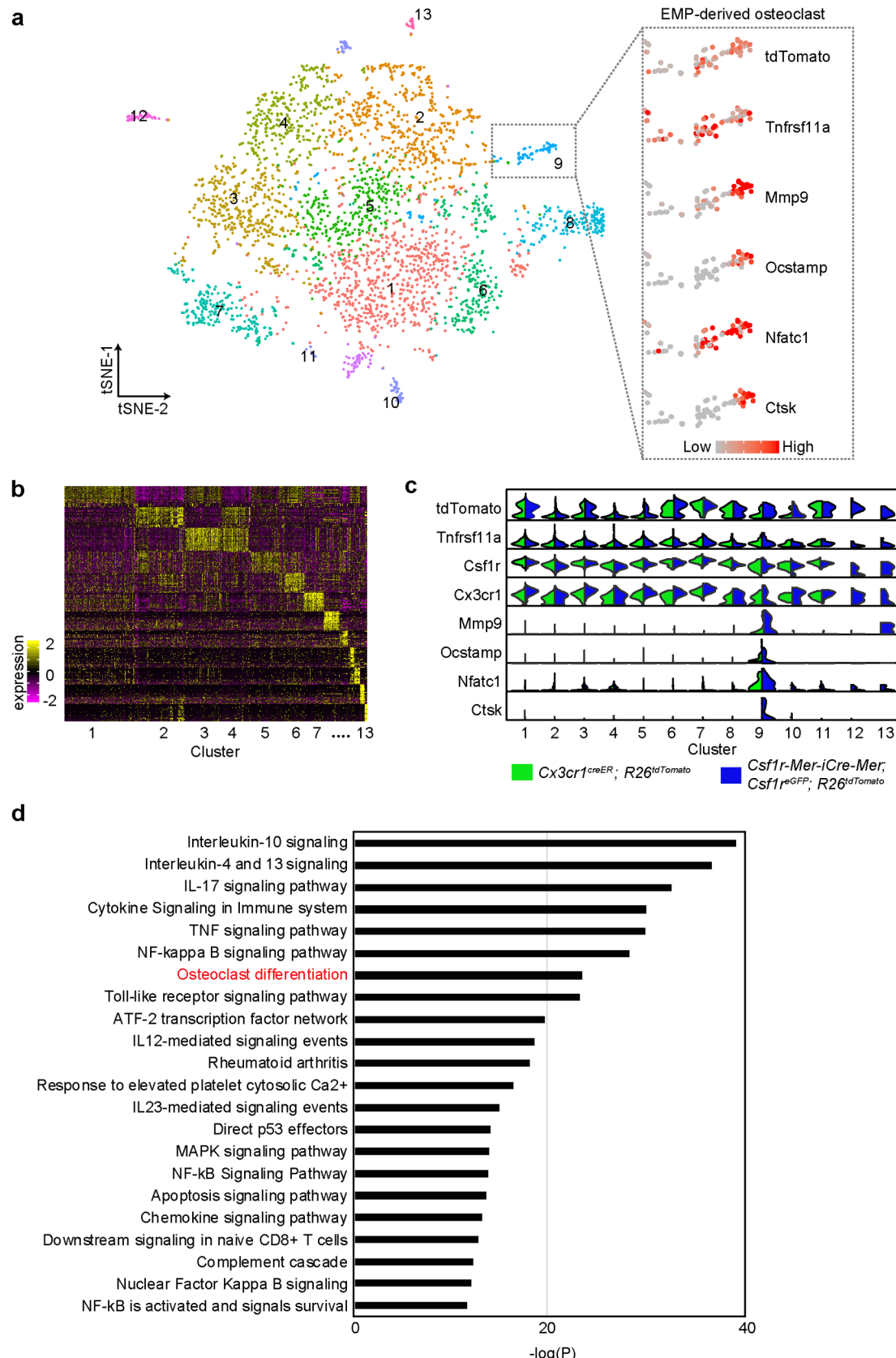
Extended Data Fig. 3 | See next page for caption.

**Extended Data Fig. 3 | Characterization of HSC- and EMP- derived cells.** **a**, Representative image of the femur of embryonic day (E) 17.5 *R26<sup>tdTomato</sup>* mice (Cre-negative littermate control of *Flt3<sup>cre</sup>*; *R26<sup>tdTomato</sup>* mice, n = 3 mice). Scale bar, 100  $\mu$ m. **b**, Relative mRNA expression levels of Cre were analyzed by quantitative PCR. RNA was isolated from adult bone marrow cells (BMCs) and E8.5 whole body. *Flt3<sup>cre</sup>*; *R26<sup>tdTomato</sup>* mice and their littermate Cre-negative control were used. **c**, Gating strategy of CD45<sup>+</sup>tdTomato<sup>+</sup> BMCs. **d**, Flow cytometry analysis of tdTomato<sup>+</sup> cells from whole-body cell suspension of E14.5 *Csf1r-Mer-iCre-Mer*; *R26<sup>tdTomato</sup>* mice labeled at E8.5 (n = 6 embryos) and *Cx3cr1<sup>creER</sup>*; *R26<sup>tdTomato</sup>* mice labeled at E9.5 (n = 5 embryos). 4OHT, 4-hydroxytamoxifen. **e**, Quantitative visualization of percentage of tdTomato<sup>+</sup> and RANK<sup>+</sup> cells from whole-body cell suspension of E14.5 *Csf1r-Mer-iCre-Mer*; *R26<sup>tdTomato</sup>* mice labeled at E8.5 (n = 6 embryos) and *Cx3cr1<sup>creER</sup>*; *R26<sup>tdTomato</sup>* mice labeled at E9.5 (n = 5 embryos). Unpaired two-tailed t-test. Error bars denote means  $\pm$  s.d. **f**, Percentage of F4/80<sup>high</sup>CD11b<sup>int</sup> macrophage and CD11b<sup>high</sup>F4/80<sup>int</sup> monocyte isolated from E14.5 whole body lysate of *Csf1r-Mer-iCre-Mer*; *R26<sup>tdTomato</sup>* mice induced at E8.5 (n = 6 embryos) and *Cx3cr1<sup>creER</sup>*; *R26<sup>tdTomato</sup>* mice induced at E9.5 (n = 5 embryos). Statistics source data are provided in Source Data Extended Data Fig. 3.



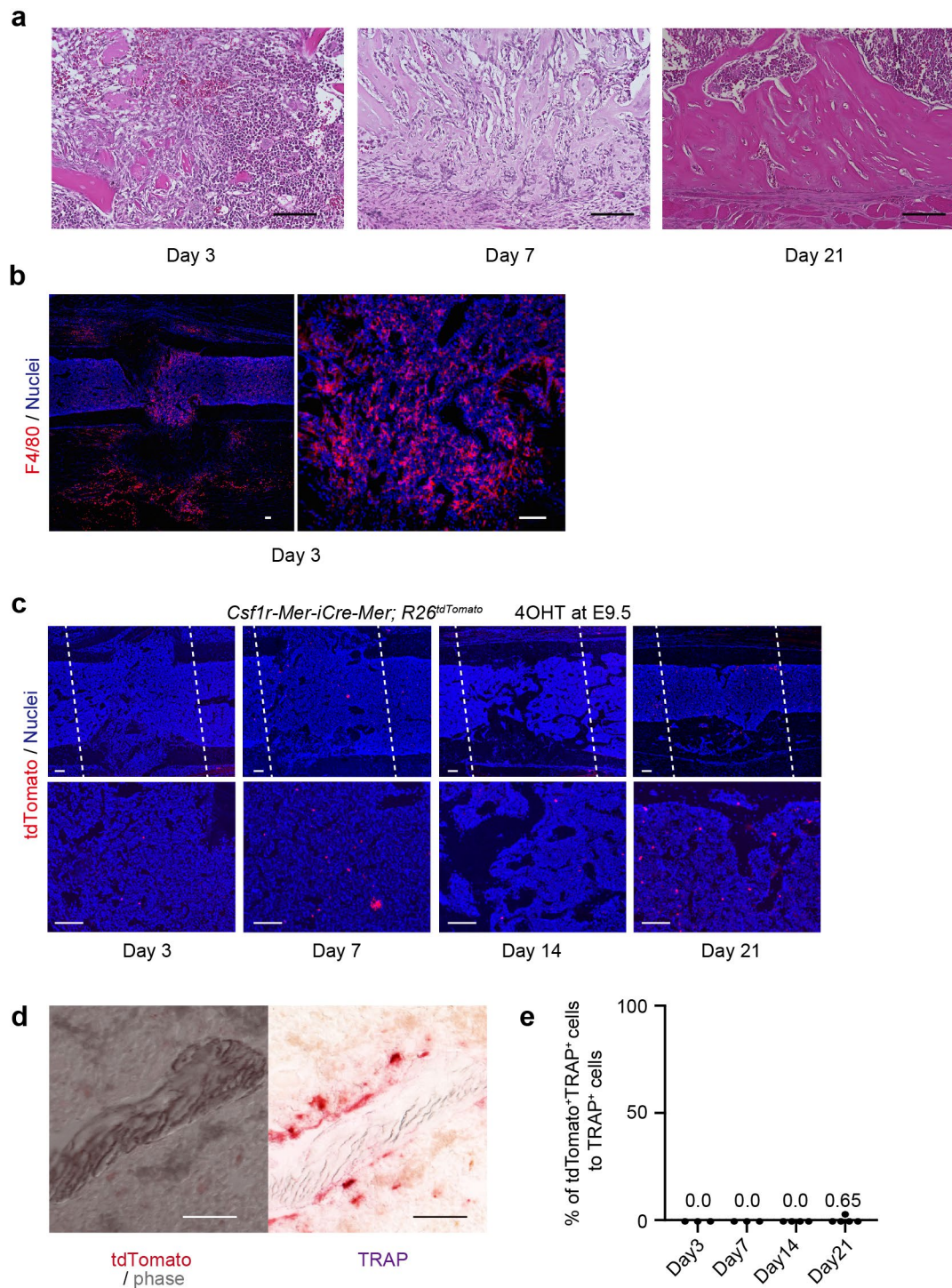
Extended Data Fig. 4 | See next page for caption.

**Extended Data Fig. 4 | Single cell RNA-sequencing analysis of E14.5 embryo.** **a**, Schematic representation of sample preparation for the single cell RNA-sequencing. 4OHT, 4-hydroxytamoxifen. **b**, Cell sorting strategy for the single cell RNA-sequencing. *tdTomato*<sup>+</sup>eGFP<sup>-</sup>, *tdTomato*<sup>+</sup>eGFP<sup>+</sup>, and *tdTomato*<sup>-</sup>eGFP<sup>+</sup> (red box) were isolated from whole-body cell suspension of *Csf1r-Mer-iCre-Mer*; *Csf1r*<sup>eGFP</sup>; *R26*<sup>tdTomato</sup> mice induced at E8.5. *tdTomato*<sup>+</sup>CX3CR1<sup>-</sup>, *tdTomato*<sup>+</sup>CX3CR1<sup>+</sup>, and *tdTomato*<sup>-</sup>CX3CR1<sup>+</sup> cell populations (green box) were also isolated from E14.5 *Cx3cr1*<sup>creER</sup>; *R26*<sup>tdTomato</sup> mice induced at E9.5. Two biological replicates of each genotype. **c**, Dot plot showing expression of the selected marker gene in each cluster of *Csf1r-Mer-iCre-Mer*; *Csf1r*<sup>eGFP</sup>; *R26*<sup>tdTomato</sup> mice. The size of the dot encodes the percentage expression, and its color encodes the average expression level. **d**, Dot plot showing expression of the selected marker gene in each cluster of *Cx3cr1*<sup>creER</sup>; *R26*<sup>tdTomato</sup> mice. **e**, Scaled expression level and frequency (the number of cells) of *tdTomato*, *Myb*, and *Flt3* were visualized. *tdTomato*<sup>+</sup> cells from *Csf1r-Mer-iCre-Mer*; *Csf1r*<sup>eGFP</sup>; *R26*<sup>tdTomato</sup> (n=10,336 cells) and *Cx3cr1*<sup>creER</sup>; *R26*<sup>tdTomato</sup> (n=6,706 cells) mice were evaluated.

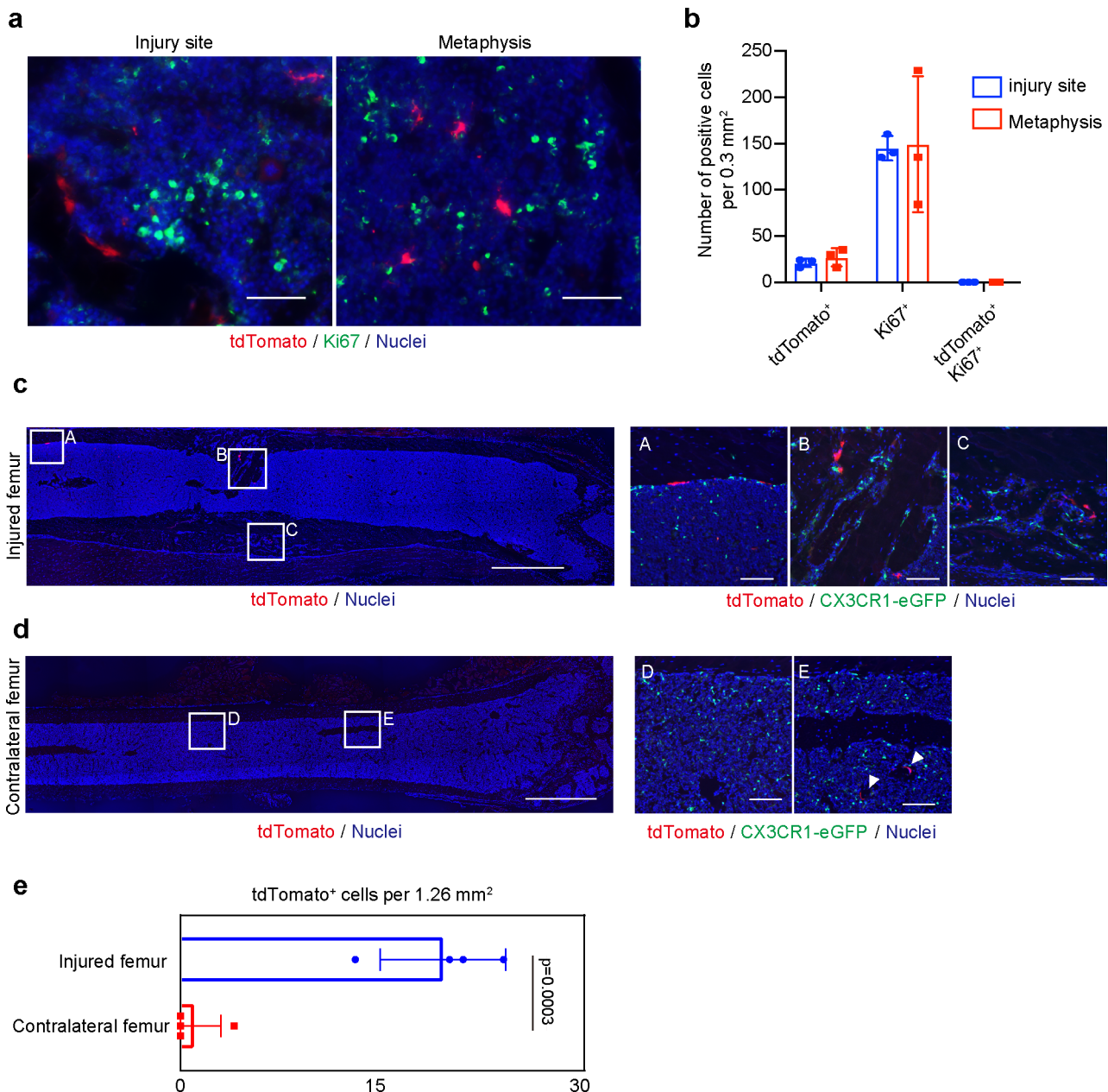


Extended Data Fig. 5 | See next page for caption.

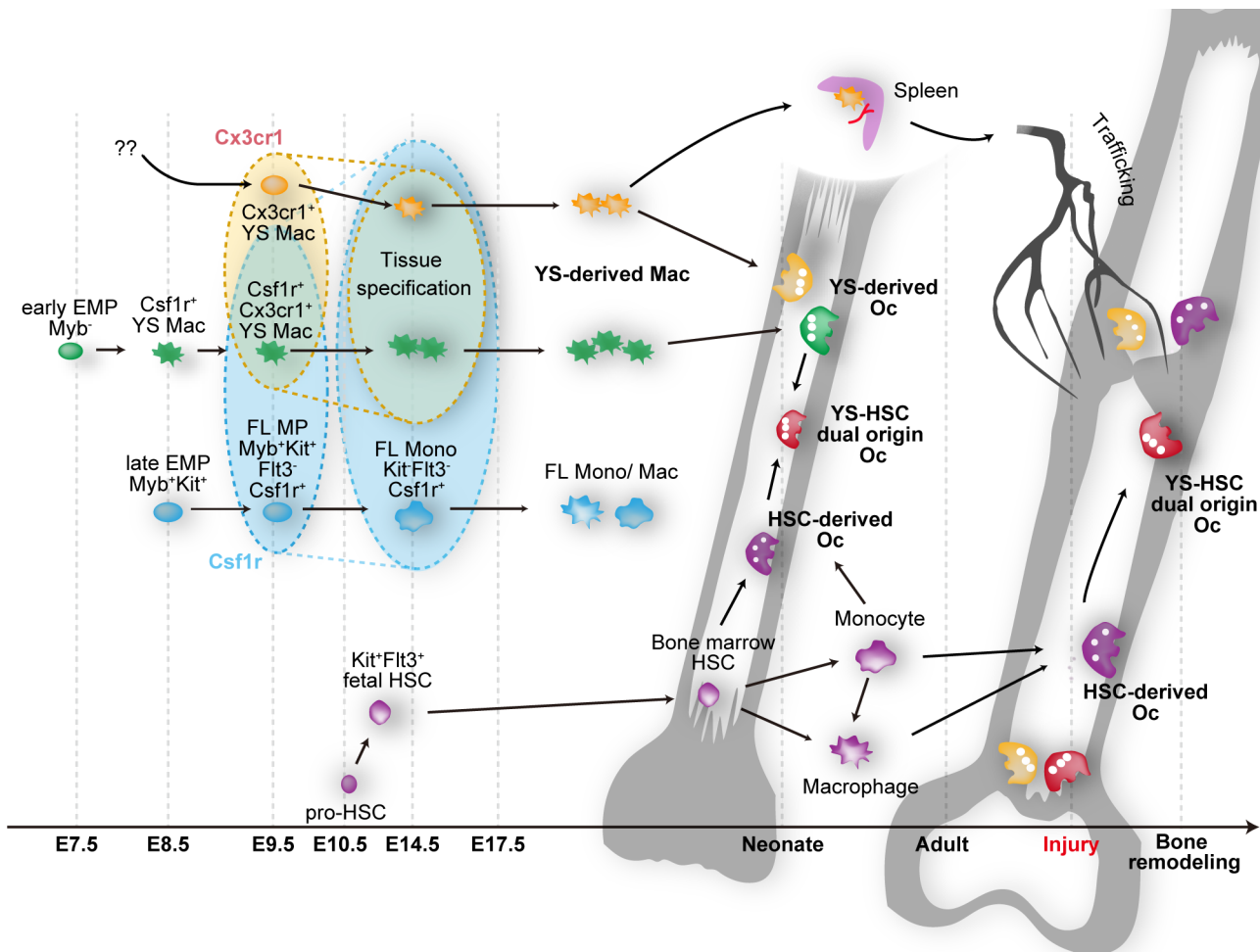
**Extended Data Fig. 5 | Single cell RNA sequencing identified EMP-derived osteoclast and their precursor populations.** **a**, t-SNE plot of  $\text{tdTomato}^+$   $\text{Tnfrsf11a}^+\text{Ptprc}^+$  cells ( $n=3,368$  cells) from  $\text{Csflr-Mer-iCre-Mer}$ ;  $\text{Csflr}^{eGFP}$ ;  $\text{R26}^{\text{tdTomato}}$  and  $\text{Cx3cr1}^{\text{creER}}\text{; R26}^{\text{tdTomato}}$  mice identifying 13 clusters. The right gray rectangle representing the normalized expression of indicated marker genes visualized onto t-SNE plots. Cells in cluster 9 expressed osteoclast-specific marker genes. EMP, erythromyeloid progenitor. **b**, Heatmap representing the top 10 significantly differentially expressed genes in each cluster. **c**, Violin plots showing mRNA expression levels of selected marker genes. Green color showing the expression levels of the cells from  $\text{Cx3cr1}^{\text{creER}}\text{; R26}^{\text{tdTomato}}$  mice. Blue color showing the expression levels of the cells from  $\text{Csflr-Mer-iCre-Mer}$ ;  $\text{Csflr}^{eGFP}$ ;  $\text{R26}^{\text{tdTomato}}$  mice. The number shows cluster identity, and the number of cells in each cluster is provided in Statistical source data Extended Data Fig 5. **d**, Selected pathways significantly enriched in the cells belonging cluster 6 ( $n=274$  cells). Hypergeometric probability mass function was used. Statistics source data are provided in source data Extended Data Fig 5.



**Extended Data Fig. 6 | The healing process of the bone injury.** **a**, Representative images of the bone injury site during the healing process. 2-month-old C57BL/6J mice received drill hole injury and were analyzed ( $n=3$  mice per group). Hematoxylin and Eosin staining showing inflammatory cells (day 3), newly synthesized bone (day 7), and regenerated bone tissue (day 21). Scale bars, 100  $\mu\text{m}$ . **b**, Immunohistochemical analysis for F4/80 expression. Representative images showing F4/80<sup>+</sup> macrophages around the injury site at day 3 ( $n=3$  mice). Scale bars, 100  $\mu\text{m}$ . **c**, Representative images of tdTomato<sup>+</sup> cells around the injury site. 2-month-old *Csf1r-Mer-iCre-Mer; R26<sup>tdTomato</sup>* mice induced with 4OHT at E9.5 received drill hole injury and were analyzed at day 3 ( $n=3$ ), 7 ( $n=3$ ), 14 ( $n=4$ ), and 21 ( $n=5$ ).  $n$  representing the number of independent animals. White dot lines represent the injury site. 4OHT, 4-hydroxytamoxifen. Scale bars, 100  $\mu\text{m}$ . **d**, Representative visualization of tdTomato<sup>+</sup> and TRAP<sup>+</sup> cells showing less contribution of tdTomato<sup>+</sup> cells to the bone remodeling at day 14 ( $n=4$  mice). Scale bars, 50  $\mu\text{m}$ . **e**, Percentage of tdTomato<sup>+</sup>TRAP<sup>+</sup> to TRAP<sup>+</sup> cells around the injury site of *Csf1r-Mer-iCre-Mer; R26<sup>tdTomato</sup>* mice at day 3 ( $n=3$ ), 7 ( $n=3$ ), 14 ( $n=4$ ), and 21 ( $n=5$ ).  $n$  representing the number of independent animals. Statistics source data are provided in Source Data Extended Data Fig. 6.



**Extended Data Fig. 7 | Migration of EMP-derived osteoclast precursors through the blood circulation.** **a**, Immunohistochemical analysis for Ki67 expression. Representative images showing Ki67<sup>+</sup> and tdTomato<sup>+</sup> cells around the injury site and adjacent metaphysis at day 14 (n=3 mice per group). Scale bars, 50  $\mu$ m. **b**, The number of single positive cells of Ki67 and tdTomato and double-positive cells per 0.3 mm<sup>2</sup> were quantified (n=3 mice per group). Error bars denote means  $\pm$  s.d. **c**, Representative images of the injured femur of *Cx3cr1eGFP/+* mice after the parabiotic union. tdTomato<sup>+</sup> cells migrated through the blood circulation at the site of a bone injury. Scale bars, 1 mm. Right panels showing enlarged images (n=4 independent parabiotic pairs). Scale bars, 100  $\mu$ m. **d**, Representative images of uninjured side femur of *Cx3cr1eGFP/+* mice. Scale bars, 1 mm. Right panels showing enlarged images (n = 4 independent parabiotic pairs). White triangles indicating tdTomato<sup>+</sup> cells. Scale bars, 100  $\mu$ m. **e**, The number of tdTomato<sup>+</sup> cells around the injury site and contralateral side of the femur. tdTomato<sup>+</sup> cells per 1.26 mm<sup>2</sup> were counted and visualized by bar chart (n = 4 mice per group). Unpaired two-tailed t-test. Error bars denote means  $\pm$  s.d. Statistics source data are provided in Source Data Extended Data Fig. 7.



**Extended Data Fig. 8 | Schematic representation showing the differential origin of osteoclast precursors and their differentiation.** Myb-independent early erythromyeloid progenitors (EMPs) appear around E7.5 in the yolk-sac and differentiate into Csf1r<sup>+</sup> yolk-sac macrophage (YS Mac) at E8.5 without passing through monocyte intermediates. YS Mac differentiates into CX3C chemokine receptor 1 (CX3CR1) positive premacrophage (pMac), resulting in a significant source of yolk-sac-derived macrophages. Late EMPs emerge in the yolk-sac at E8.5 and migrate to the fetal liver to produce Myb-expressing fetal liver (FL) myeloid progenitors (MP), resulting in FL monocyte (FL Mono). Hematopoietic stem cell precursors (pro-HSCs) emerge at E10.5. Pro-HSCs migrate to the fetal liver around E12 and turns to fetal HSCs, which later shift to the bone marrow. Bone marrow HSCs eventually can establish the circulating monocyte-derived macrophages. YS-derived macrophages differentiate into osteoclast (YS-derived Oc) in the neonatal bone with possible cell-cell fusion with HSC-derived Oc precursors. Cx3cr1<sup>+</sup> yolk-sac macrophage descendants in the spleen can provide long-lasting Oc that contribute to the postnatal bone remodeling after injury via the bloodstream.

Corresponding author(s): Benjamin Alman

Last updated by author(s): Oct 21, 2019

## Reporting Summary

Nature Research wishes to improve the reproducibility of the work that we publish. This form provides structure for consistency and transparency in reporting. For further information on Nature Research policies, see [Authors & Referees](#) and the [Editorial Policy Checklist](#).

### Statistics

For all statistical analyses, confirm that the following items are present in the figure legend, table legend, main text, or Methods section.

n/a Confirmed

- The exact sample size ( $n$ ) for each experimental group/condition, given as a discrete number and unit of measurement
- A statement on whether measurements were taken from distinct samples or whether the same sample was measured repeatedly
- The statistical test(s) used AND whether they are one- or two-sided  
*Only common tests should be described solely by name; describe more complex techniques in the Methods section.*
- A description of all covariates tested
- A description of any assumptions or corrections, such as tests of normality and adjustment for multiple comparisons
- A full description of the statistical parameters including central tendency (e.g. means) or other basic estimates (e.g. regression coefficient) AND variation (e.g. standard deviation) or associated estimates of uncertainty (e.g. confidence intervals)
- For null hypothesis testing, the test statistic (e.g.  $F$ ,  $t$ ,  $r$ ) with confidence intervals, effect sizes, degrees of freedom and  $P$  value noted  
*Give  $P$  values as exact values whenever suitable.*
- For Bayesian analysis, information on the choice of priors and Markov chain Monte Carlo settings
- For hierarchical and complex designs, identification of the appropriate level for tests and full reporting of outcomes
- Estimates of effect sizes (e.g. Cohen's  $d$ , Pearson's  $r$ ), indicating how they were calculated

*Our web collection on [statistics for biologists](#) contains articles on many of the points above.*

### Software and code

Policy information about [availability of computer code](#)

#### Data collection

Images were captured using Axio Imager Z2 Widefield Fluorescence Microscope (Zeiss), IX-83 (OLYMPUS), and BZ-9000 Biorevo microscope (Keyence). To generate single cell cDNA library, 10x Genomics Chromium Controller Single-Cell Instrument (10x Genomics) were used. Sequencing libraries were transferred to the Duke University Center for Genomic and Computational Biology (GCB) and were loaded on a Novaseq 6000 (Illumina) for sequencing. qPCR was performed using QuantStudio 3 real-time PCR system (Thermo Fisher Scientific). For uCT analysis, VivaCT 80 (Scanco Medical AG) was used.

#### Data analysis

GraphPad Prism7 (version 7.0d), Statcel ver 3.0 (OMS), and Microsoft Excel2016 were used for statistical analysis. Data of flow cytometry were analyzed by FlowJo version 10 (Tree Star). Images were analyzed using ImageJ bundled with 64-bit Java 1.8.0\_112 (NIH), and Zen 2.3 software (Zeiss). To quantify the number of tdTomato+TRAP+ cells, images were merged using Photoshop ver 20.0.6 and Illustrator ver 23.0.6 (Adobe).  
The primary analytical pipeline for the single cell analysis followed the recommended protocols from 10X Genomics. Briefly, we processed the raw FASTQ files using the Cell Ranger software version 3.0. The secondary statistical analysis was performed using R version 3.5.3 and Seurat version 3.0.0.9000 (<http://satijalab.org/seurat/>). ToppGene suite (<https://toppgene.cchmc.org/help/publications.jsp>) used for pathway analysis.

For manuscripts utilizing custom algorithms or software that are central to the research but not yet described in published literature, software must be made available to editors/reviewers. We strongly encourage code deposition in a community repository (e.g. GitHub). See the Nature Research [guidelines for submitting code & software](#) for further information.

## Data

Policy information about [availability of data](#)

All manuscripts must include a [data availability statement](#). This statement should provide the following information, where applicable:

- Accession codes, unique identifiers, or web links for publicly available datasets
- A list of figures that have associated raw data
- A description of any restrictions on data availability

Single cell RNA sequencing data that support the findings of this study have been deposited in the Gene Expression Omnibus (GEO) under accession cod: GSE125088. Source data have been provided as Statistical source data Fig. 1-6 and Statistical source data Extended data Fig. 3, 5, 6, and 7. All other data supporting the findings of this study are available from the corresponding author on reasonable request.

## Field-specific reporting

Please select the one below that is the best fit for your research. If you are not sure, read the appropriate sections before making your selection.

Life sciences       Behavioural & social sciences       Ecological, evolutionary & environmental sciences

For a reference copy of the document with all sections, see [nature.com/documents/nr-reporting-summary-flat.pdf](https://nature.com/documents/nr-reporting-summary-flat.pdf)

## Life sciences study design

All studies must disclose on these points even when the disclosure is negative.

Sample size	Sample size was determined accordingly to previous published study and experimental knowledge (Jacome-Galarza CE et al., Nature 2019, Romeo SG et al., Nat Cell Biol. 2019). No statistical methods were used to predetermine sample size.
Data exclusions	In bone injury experiment, mice have dislocated femur fracture were excluded because of excessive fracture callus formation. Because we only focused on the healing process of drill hole injury of femur, but not totally fractured bone. Mice have dislocated femur fracture were euthanized after surgery. There are no pre-established exclusion criteria. For neonatal mice analysis, stillbirth pups were excluded. Because tamoxifen induction in pregnant female cause unpredictable abortion or stillbirth. In other experiments, no data were excluded from the analysis.
Replication	Analyses of the single cell RNA-seq were performed in 2 biological replicates of each genotype. Another experiments were performed in at least n=3 independent biological samples.
Randomization	Samples were allocated randomly into experimental groups and time point analysis.
Blinding	No blinding were used in this study and it was not possible. For the lineage tracing and parabiosis experiments, pregnant female were injected with tamoxifen and sometime it caused toxicity. Investigator need to monitor and record animal condition and access to the mouse data.

## Reporting for specific materials, systems and methods

We require information from authors about some types of materials, experimental systems and methods used in many studies. Here, indicate whether each material, system or method listed is relevant to your study. If you are not sure if a list item applies to your research, read the appropriate section before selecting a response.

### Materials & experimental systems

n/a	Involved in the study
<input type="checkbox"/>	<input checked="" type="checkbox"/> Antibodies
<input checked="" type="checkbox"/>	<input type="checkbox"/> Eukaryotic cell lines
<input checked="" type="checkbox"/>	<input type="checkbox"/> Palaeontology
<input type="checkbox"/>	<input checked="" type="checkbox"/> Animals and other organisms
<input checked="" type="checkbox"/>	<input type="checkbox"/> Human research participants
<input checked="" type="checkbox"/>	<input type="checkbox"/> Clinical data

### Methods

n/a	Involved in the study
<input checked="" type="checkbox"/>	<input type="checkbox"/> ChIP-seq
<input type="checkbox"/>	<input checked="" type="checkbox"/> Flow cytometry
<input checked="" type="checkbox"/>	<input type="checkbox"/> MRI-based neuroimaging

## Antibodies

### Antibodies used

For flow cytometry, the following antibodies were used:  
 APC-Cy™7 Rat Anti-CD11b Clone M1/70 (BD Biosciences, catalog#; 561039, lot#, 7278811, 1:100)  
 Alexa Fluor® 647 Rat Anti-Mouse F4/80 (BD Biosciences, catalog#; 565854, lot#, 7178647, 1:100)  
 FITC Rat Anti-Mouse CD45 Clone 30-F11 (BD Biosciences, catalog#; 561088, lot#, 8206667, 1:100)  
 PE-Cy™7 Rat Anti-Mouse CD45 BD (Biosciences, catalog#; 552848, lot#, 8116600, 1:100)

FITC anti-mouse CX3CR1 Antibody (BioLegend, catalog#; 149020, lot#; B229602, 1:100)  
 Purified Rat Anti-Mouse CD16/CD32 (BD Biosciences, catalog#; 553142, lot#; 8130843, 1:100)  
 Alexa Fluor® 647 Mouse Anti-RANK (CD265) (BD Biosciences, catalog#; 566348, lot#; 7045934, 1:100)  
 7-AAD (BD Biosciences, catalog#; 559925, lot#; 8299804, )

For immunostaining, the following antibodies were used:  
 F4/ 80 antibody Cl: A3-1 (BIORAD, catalog#; MCA497R, lot#; 1610, 1:200)  
 Ki-67 Monoclonal Antibody (SolA15) (Thermo Fisher Scientific, catalog#; 14-5698-82, lot#; 2002315, 1:200)  
 Anti-ATP6V1B1 + ATP6V1B2 (Abcam, catalog#; ab200839, lot#; GR3250372-3, 1:200)  
 RFP Antibody Pre-adsorbed (Rockland, catalog#; 600-401-379, lot#; 38544, 1:500)  
 Goat anti-Rat IgG (H+L) Cross-Adsorbed Secondary Antibody, Alexa Fluor 647 (Thermo Fisher Scientific, catalog#; A-21247, lot#; 1858181, 1:2000)  
 Goat anti-Rabbit IgG (H+L) Superclonal™ Secondary Antibody, Alexa Fluor 488 (Thermo Fisher Scientific, catalog#; A27034, lot#; 1670152, 1:2000)  
 Hoechst 33342, Trihydrochloride, Trihydrate, 100 mg (Thermo Fisher Scientific, catalog#; H1399, lot#; RD234403, 1:2000)

## Validation

We used primary antibodies according to the manufacturers instruction, and confirmed similar results with validation results on manufacturer's website or relevant citations.

APC-Cy™7 Rat Anti-CD11b Clone M1/70 (BD Biosciences, catalog#; 561039) antibody has been validated by the manufacturer (<https://www.bd-biosciences.com/eu/applications/research/stem-cell-research/mesenchymal-stem-cell-markers/bone-marrow/human/negative-markers/apc-cy7-rat-anti-cd11b-m170/p/561039>)  
 Alexa Fluor® 647 Rat Anti-Mouse F4/80 (BD Biosciences, catalog#; 565854) antibody has been validated by the manufacturer (<https://www.bd-biosciences.com/ca/reagents/research/antibodies-buffers/immunology-reagents/anti-mouse-antibodies/cell-surface-antigens/alexa-fluor-647-rat-anti-mouse-f480-t45-2342/p/565854>)  
 FITC Rat Anti-Mouse CD45 Clone 30-F11 (BD Biosciences, catalog#; 561088) antibody has been validated by the manufacturer (<https://www.bd-biosciences.com/us/applications/research/stem-cell-research/cancer-research/mouse/fitc-rat-anti-mouse-cd45-30-f11/p/561088>)  
 PE-Cy™7 Rat Anti-Mouse CD45 BD (Biosciences, catalog#; 552848) antibody has been validated by the manufacturer (<https://www.bd-biosciences.com/eu/applications/research/stem-cell-research/cancer-research/mouse/pe-cy7-rat-anti-mouse-cd45-30-f11/p/552848>)  
 FITC anti-mouse CX3CR1 Antibody (BioLegend, catalog#; 149020) has been validated by the manufacturer (<https://www.biolegend.com/en-us/products/fitc-anti-mouse-cx3cr1-antibody-11878>)  
 Purified Rat Anti-Mouse CD16/CD32 (BD Biosciences, catalog#; 553142) antibody has been validated by the manufacturer (<https://www.bd-biosciences.com/us/applications/research/b-cell-research/surface-markers/mouse/purified-rat-anti-mouse-cd16cd32-mouse-bd-fc-block-24g2/p/553142>)  
 Alexa Fluor® 647 Mouse Anti-RANK (CD265) antibody (BD Biosciences, catalog#; 566348) has been validated by the manufacturer (<https://www.bd-biosciences.com/us/reagents/research/antibodies-buffers/immunology-reagents/anti-mouse-antibodies/cell-surface-antigens/alexa-fluor-647-mouse-anti-rank-cd265-9a725/p/566348>)  
 F4/ 80 antibody Cl: A3-1 antibody (BIORAD, catalog#; MCA497R) has been validated by the manufacturer (<https://www.bio-rad-antibodies.com/monoclonal/mouse-f4-80-antibody-cl-a3-1-mca497.html?f=purified>)  
 Ki-67 Monoclonal Antibody antibody (Thermo Fisher Scientific, catalog#; 14-5698-82) has been validated by Jurisevic M et al., Oncotarget. 2018.  
 Anti-ATP6V1B1 + ATP6V1B2 (Abcam, catalog#; ab200839) antibody has been validated by Romeo SG et al., Nat cell biol 2019.  
 RFP Antibody Pre-adsorbed (Rockland, catalog#; 600-401-379) antibody has been validated by the manufacturer ([https://rockland-inc.com/store/Antibodies-to-GFP-and-Antibodies-to-RFP-600-401-379-O4L\\_24299.aspx](https://rockland-inc.com/store/Antibodies-to-GFP-and-Antibodies-to-RFP-600-401-379-O4L_24299.aspx))

## Animals and other organisms

Policy information about [studies involving animals](#); [ARRIVE guidelines](#) recommended for reporting animal research

### Laboratory animals

Csf1r-Mer-iCre-Mer (FVB-Tg(Csf1r-cre/Esr1\*)1Jwp/J), Cx3cr1CreER (B6.129P2(C)-Cx3cr1tm2.1(cre/ERT2)Jung/J ), R26tdTomato (B6.Cg-Gt(ROSA)26Sor tm14(CAG-tdTomato)Hze/J), Csf1r-EGFP (C57BL/6-Tg(Csf1r-EGFP-NGFR/FKBP1A/TNFRSF6)2Bck/J), Cx3cr1EGFP (B6.129P-Cx3cr1tm1Litt/J), and C57BL/6J, Flt3-Cre mice were used for this research. For lineage tracing experiment, pregnant female mice were injected with 4OH-tamoxifen at E8.5 or 9.5. E14.5 female and male pups were used for single cell RNA sequencing analysis and cell culture. Both male and female mice from fetal to postnatal stages were analyzed (E17.5 to 6 month old). For parabiosis experiments, 2-month-old Cx3cr1CreER female mice and Cx3cr1EGFP female mice were used.

### Wild animals

The study did not involve wild animals.

### Field-collected samples

This study did not involve any field-collected samples.

### Ethics oversight

All animals were used according to the approved protocol by the Institutional Animal Care and Use Committee of Duke University.

Note that full information on the approval of the study protocol must also be provided in the manuscript.

# Flow Cytometry

## Plots

Confirm that:

- The axis labels state the marker and fluorochrome used (e.g. CD4-FITC).
- The axis scales are clearly visible. Include numbers along axes only for bottom left plot of group (a 'group' is an analysis of identical markers).
- All plots are contour plots with outliers or pseudocolor plots.
- A numerical value for number of cells or percentage (with statistics) is provided.

## Methodology

### Sample preparation

To obtain single cell suspension from E14.5 embryos, pregnant females were euthanized by exposure to CO<sub>2</sub>. Embryos were collected from the uterus and washed with PBS. Each embryo was minced by a scalpel, and then digested with Collagenase type 4 (200 units per mg weight, Worthington), 200 U ml<sup>-1</sup> DNase I (Sigma Aldrich) in 1% Bovine serum albumin (BSA, Sigma)/PBS for 20 minutes at 37 °C. The whole-body cell suspension was filtered by 70- and 30-µm cell strainer. To obtain the bone marrow cells (BMCs), 0.5-, 2-, and 6-month-old mice tibia were used. Bilateral tibia were dissected, and the distal/ proximal end of the tibia were removed. BMCs were then collected and mechanically dissociated to make a single cell suspension. BMCs were filtered by 40-µm cell strainer.

### Instrument

Flow cytometry was performed with a FACSCanto II flow cytometer (BD Biosciences). For cell sorting, a DiVa cell sorter (BD Biosciences) was used.

### Software

Data were analyzed by FlowJo 10 (Tree Star).

### Cell population abundance

About 100,000 tdTomato+ cells were isolated from one Csfr1r-Mer-iCre-Mer; R26tdTomato embryo induced with 4 hydroxytamoxifen at E8.5. About 20,000 tdTomato+ cells were isolated from one Cx3cr1CreER; R26tdTomato embryo induced with 4 hydroxytamoxifen at E9.5. About 200,000 bone marrow cells expressing EGFP were isolated from one Csfr1r-EGFP mice. Those cell were subjected to single cell RNA sequencing, cell culture, and RNA extraction.

### Gating strategy

FSC-A/ SSC-A and FSC-H/ FSC-A gating were used to excluding debris and doublet cells. Detail gating strategy is provided in the Extended data Fig3c and Extended data Fig4b.

- Tick this box to confirm that a figure exemplifying the gating strategy is provided in the Supplementary Information.